Accurate Modeling of Optical Multiplexer/Demultiplexer Concatenation in Transparent Multiwavelength Optical Networks

I. Roudas, *Member, IEEE*, N. Antoniades, *Member, IEEE*, T. Otani, T. E. Stern, *Life Fellow, IEEE*, R. E. Wagner, *Member, IEEE*, and D. Q. Chowdhury, *Member, IEEE*

***Abstract*—This paper presents an accurate theoretical model for the study of concatenation of optical multiplexers/demultiplexers (MUXs/DMUXs) in transparent multiwavelength optical networks. The model is based on a semianalytical technique for the evaluation of the error probability of the network topology. The error-probability evaluation takes into account arbitrary pulse shapes, arbitrary optical MUX/DMUX, and electronic low-pass filter transfer functions, and non-Gaussian photocurrent statistics at the output of the direct-detection receiver. To illustrate the model, the cascadability of arrayed waveguide grating (AWG) routers in a transparent network element chain is studied. The performance of the actual network is compared to the performance of a reference network with ideal optical MUXs/DMUXs. The optical power penalty at an error probability of 10^{-9} is calculated as a function of the number of cascaded AWG routers, the bandwidth of AWG routers, and the laser carrier frequency offset from the channel's nominal frequency.**

***Index Terms*—Error analysis, optical filters, optical receivers.**

I. Introduction

IN TRANSPARENT multiwavelength optical networks, each lightwave signal may be optically multiplexed/demultiplexed several times during propagation from its source to its destination [1]. Optical multiplexers/demultiplexers (MUXs/DMUXs) exhibit nonideal amplitude and phase transfer functions within the optical signal band. That is, their amplitude transfer functions might present passband curvature, tilt, and ripple. In addition, their phase transfer functions might not vary linearly with frequency. These impairments are enhanced when a large number of these devices are cascaded together. Consequently, optical MUX/DMUX concatenation causes signal attenuation and distortion, i.e., intersymbol interference (ISI), and eventually limits the maximum number of optical network elements that can be cascaded.

In the past, the cascadability of different types of optical MUXs/DMUXs was studied both theoretically [2]–[18] and experimentally [11], [18]–[24] for several bit rates, channel spacings, modulation formats, and other system considerations. Most attention was concentrated on arrayed waveguide grating (AWG) routers [6], [11], [13], [17], [19]–[22], [24], MUXs/DMUXs composed of multilayer interference (MI) filters [4], [5], [8], [10], [14], [17], [18], and MUXs/DMUXs composed of fiber Bragg grating filters [14], [15], [23]. General studies, not bound to a specific optical MUX/DMUX type, but based on arbitrary transfer functions, also exist, e.g., [7] and [16].

Previous theoretical studies contain approximations concerning the network topology and the network performance evaluation. More specifically, [4]–[6], [9], [10], and [12]–[18] study isolated chains of optical MUXs/DMUXs instead of realistic network topologies. In the latter case, the signal spectral clipping due to the concatenation of optical MUXs/DMUXs introduces an excess loss which changes the operating point of optical servo-controlled attenuators and erbium-doped fiber amplifiers (EDFAs) in the network elements. Therefore, it is necessary to study the interaction between optical MUXs/DMUXs, optical servo-controlled attenuators and EDFAs, and its impact on the power levels of the optical signal and amplified spontaneous emission (ASE) noise in the network.

In addition, little effort was devoted to evaluate accurately the network performance degradation due to the concatenation of optical MUXs/DMUXs. References [2], [4], [5], [7], [9], [10], [12]–[14], [16], and [17] compute the eye pattern at the output of the direct-detection receiver by noiseless simulation and use the eye opening as a qualitative criterion of the network performance. Other authors [3], [6], [8], [11], [18] include ASE noise in their calculation with various degrees of accuracy, but assume Gaussian receiver noise statistics at the output of the direct-detection receiver. This assumption is strictly valid only for thermal-noise-limited receivers, but not for the most common case of optically preamplified direct-detection receivers.

This paper presents an accurate theoretical model, free of both aforementioned limitations, for the study of the concatenation of optical MUXs/DMUXs in transparent multiwavelength optical networks. The key features of the proposed model are

Manuscript received May 4, 2001; revised February 21, 2002. This work was supported by the Defense Advanced Research Projects Agency under MDA 972-95-3-0027 and performed as a part of the MONET consortium.

I. Roudas was with the Telcordia Technologies, Red Bank, NJ 07701 USA. He is now with Corning Inc., Somerset, NJ 08873 USA.

N. Antoniades was with the with the Department of Electrical Engineering, Columbia University, New York, NY 10027 USA. He is now with Corning Inc., Somerset, NJ 08873 USA.

T. Otani was with the Department of Electrical Engineering, Columbia University, New York, NY 10027 USA. He is now with the KDD Research and Development Laboratories, Saitama 356-8502, Japan.

T. E. Stern is with the Department of Electrical Engineering, Columbia University, New York, NY 10027 USA.

R. E. Wagner was with the Telcordia Technologies, Red Bank, NJ 07701 USA. He is now with Corning Inc., Corning, NY 14831 USA.

D. Q. Chowdhury is with Corning Inc., Corning, NY 14831 USA.

Publisher Item Identifier S 0733-8724(02)05399-9.

the following: 1) it is based on a transparent chain of wavelength add-drop multiplexers (WADMs) or wavelength selective cross-connects (WSXCs) and 2) it uses the error probability as a criterion for the cascadability of optical MUXs/DMUXs in the network. The error-probability evaluation takes into account arbitrary pulse shapes, arbitrary optical MUXs/DMUXs and electronic low-pass filter (LPF) transfer functions, and non-Gaussian photocurrent statistics at the output of the direct-detection receiver. For the error-probability evaluation, the model combines a semianalytic method [25] with an accurate statistical analysis of square-law detection [26]–[41]. The computation involves several steps, including expansion of the ASE noise impingent upon the photodiode in Karhunen–Loève series [42]–[44], numerical solution of the associated homogeneous Fredholm equation of the second kind [44]–[46], diagonalization of a quadratic form [37], [45], and asymptotic evaluation of the probability density function (pdf) at the output of the direct-detection receiver from the characteristic function using the method of steepest descent [26], [38], [41], [46].

To illustrate the model, the concatenation of AWG routers in a transparent network element chain is studied. The error probability is calculated as a function of the number of AWG routers, the optical bandwidth of AWG routers, and the laser carrier frequency offset from the channel's nominal frequency. These results are compared to the performance of a reference network composed of optical MUXs/DMUXs with rectangular amplitude response and zero phase response.

The following conclusions are drawn.

1) It is possible to concatenate an arbitrary number of conventional AWG routers, despite the inherent passband curvature of these devices, by increasing the equivalent noise bandwidth of individual AWG routers for a given bit rate at the expense of channel spacing.
2) In the case that the equivalent noise bandwidth of the individual AWG routers is much larger than the bit rate, when the number of cascaded AWG routers increases, initially the network performance is improved because the optical bandwidth narrowing due to AWG router concatenation reduces the power of the ASE noise at the direct-detection receiver without essentially distorting the signal. As the number of cascaded AWG routers continues to increase, the effective equivalent noise bandwidth of the AWG router cascade becomes comparable to the bit rate and the network performance slowly degrades due to the increase of ISI.
3) Using the current model, it is possible in principle to maximize the network performance for a given number of concatenated AWG routers by jointly optimizing the optical bandwidth of the individual AWG routers and the electronic bandwidth of the receiver.
4) Finally, for narrow optical MUX/DMUX bandwidths, the network performance can be maximized by misaligning the laser carrier frequency from the optical MUXs/DMUXs center frequency.

The rest of the paper is organized as follows. Section II presents the theoretical model for the study of concatenation of optical MUXs/DMUXs in transparent multiwavelength optical networks. Section III presents a study case for the concatenation of AWG routers in a chain of transparent network elements. The details of the calculations are given in Appendixes A–C.

II. Theoretical Model

This section is divided into five parts. The first topic that is treated is the representation of an optical network topology by two separate equivalent channels for the signal and the ASE noise, respectively. For illustrative purposes and without loss of generality, a chain of optical network elements is studied, since it is the elementary building block of more complex network topologies. In addition, a reference network is defined and is used for comparison with the actual network.

The second topic of this section is the mathematical description for the signal and ASE noise propagation through their equivalent channels and the derivation of an analytical expression for the photocurrent at the output of the direct-detection receiver. This treatment highlights the underlying mechanisms for performance degradation and provides a rigorous definition for the excess loss resulting from the optical MUXs/DMUXs. In addition, we introduce the notion of the excess noise factor, originating from a decrease in the insertion loss of servo-controlled optical attenuators.

The third topic of this section is the evaluation of the statistics of the photocurrent at the output of the direct-detection receiver. The fourth topic of this section is the description of the semianalytical method for the evaluation of the average error probability. The fifth topic of this section is the derivation of an analytical expression for the error probability of the reference network. We begin our discussion with a description of the network topology.

A. Network Representation

The network topology is shown in Fig. 1(a). It consists of a chain of $M+1$ equidistant network elements separated by M fiber spans of loss L. All fibers carry wavelength division multiplexed (WDM) optical signals. One optical signal, at nominal carrier frequency f_s, is added at the first network element and propagates through the entire chain (dotted line).

An exhaustive study of network element architectures is beyond the scope of this paper. Fig. 1(b) shows an example architecture of a reconfigurable WADM proposed in the multiwavelength optical networking (MONET) project [47]. It consists of two EDFAs, an optical MUX/DMUX pair, an optical switch fabric for signal adding/dropping, and servo-controlled attenuators for power equalization. An example architecture of an eight wavelength 4×4 WSXC can be found in [48]. It can be shown that in the WSXC the optical signal passes from the same number of optical components as shown in Fig. 1(b).

The optical transmitter and receiver, notionally, are not parts of the optical transport layer [1], so they are not included in Fig. 1(b). Fig. 1(c) shows the structure of an optically preamplified direct-detection receiver. The EDFA at the input of the $(M+1)$th network element is playing the role of the receiver optical preamplifier and is omitted in Fig. 1(c). The remainder of the receiver consists of a polarizer (optional), a tunable optical

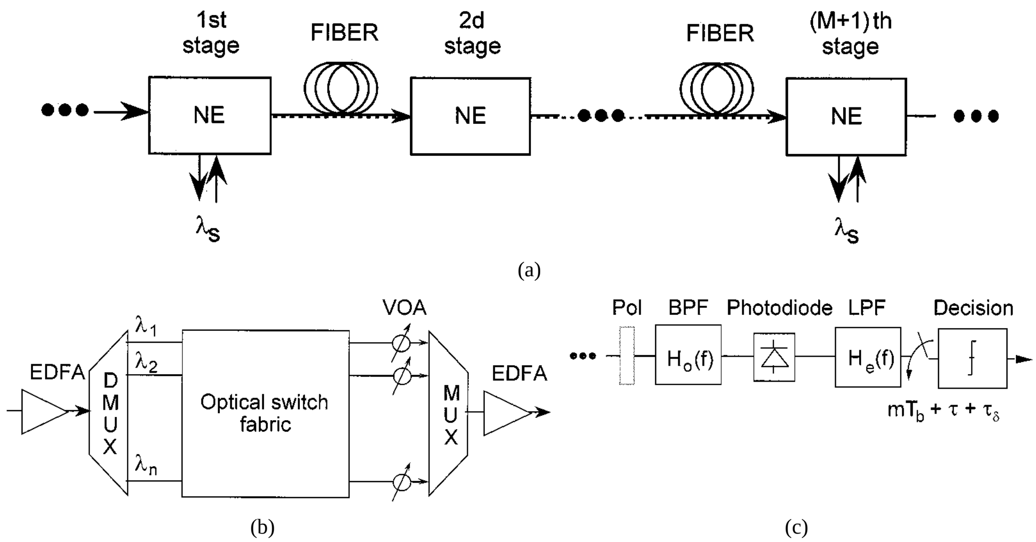

Fig. 1. (a) Chain network topology. Dotted line indicates the optical path of the signal under study (NE: network element; λ_s: signal's nominal carrier wavelength). (b) Architecture of a WADM (EDFA: Erbium-doped fiber amplifier; DMUX: demultiplexer; MUX: multiplexer; VOA: servo-controlled attenuator). (c) Block diagram of an optically preamplified direct-detection receiver (Pol: Polarizer; BPF: tunable optical BPF with low-pass equivalent transfer function denoted by $H_o(f)$; LPF: electronic low-pass filter with transfer function denoted by $H_e(f)$; T_b: bit period; τ propagation delay; τ_δ: sampling instant).

bandpass filter (BPF) with transfer function denoted by $H_o(f)$, a photodiode, an electronic LPF with transfer function denoted by $H_e(f)$, a sampler, and a decision device, whose threshold is automatically set to minimize the error probability. The signal is sampled at times $t_m = mT_b + \tau + \tau_\delta$, where $m \in N$, T_b is the bit period, τ is the propagation group delay through the network, and $\tau_\delta \in [0, T_b)$ is the specific sampling position within the bit that minimizes the error probability.

For simplicity, we consider the case of single channel transmission. It is assumed that signal attenuation induced by the optical fibers is compensated fully by the EDFAs at the input of the network elements. The generalization to the case when the signal attenuation induced by the optical fibers is not compensated fully by the EDFAs at the input of the network elements (e.g., in the case of WDM transmission and EDFA gain ripple) is straightforward. Signal attenuation within the network elements arises from the insertion loss of the optical components and the band-limiting operation of the optical MUXs/DMUXs. To isolate the impact of the filtering by the optical MUXs/DMUXs, we assume that the network elements are designed so that the EDFAs at the output of each network element compensate fully the total intranode insertion loss, if the optical MUXs/DMUXs are replaced by optical attenuators with the same insertion loss as the optical MUXs/DMUXs exhibit at their center frequency. Any additional signal attenuation caused by signal filtering by the optical MUXs/DMUXs is defined as excess loss [4]. The excess loss is compensated by adjusting the insertion loss of the servo-controlled attenuator following the MUX/DMUX pair in order to keep the average signal power at the input of the booster EDFA constant. Without loss of generality, it is assumed that the excess loss per node is within the operating range of the servo-controlled attenuators.

The above assumptions enable the reduction of the network topology to the simplified block diagram shown in Fig. 2(a). All intranode optical components and fibers from the initial Fig. 1(a) and (b) is eliminated.[1] Optical MUXs/DMUXs are represented by filters with transfer functions normalized to unity and denoted by $H_i(f)$, $i = 1, \ldots, 2M$. The receiver tunable optical BPF with transfer function $H_o(f)$ is also included. The servo-controlled attenuators are represented by gain elements with gain g_i, $i = 1, \ldots, M$, equal to the excess loss caused by the optical MUX/DMUX pair of the ith node. The EDFAs are represented by independent white Gaussian noise sources $n_{\mathrm{eq},i}(t)$, $i = 1, \ldots, 2M$. The electric fields at the output of the transmitter and the input of the receiver are denoted by $E_s(t)$ and $E(t)$, respectively.

Inspection of the simplified block diagram shown in Fig. 2(a) reveals that the signal passes through $2M$ MUXs/DMUXs and M servo-controlled attenuators, which compensate for the excess loss caused by the first $2M - 1$ MUXs/DMUXs, but not for the excess loss resulting from the $2M$th DMUX at the drop site. Consequently, the excess loss cannot be fully compensated as assumed by previous authors [4], [5].

The ASE noise generated by the $2M$ EDFAs is amplified by the effective gain provided by the last $M - 1$ servo-controlled attenuators and is filtered by the last $2M - 1$ MUXs/DMUXs. The effective gain provided by the servo-controlled attenuators in the ASE noise path causes an additional ASE noise amplification. This effect is described by an excess noise factor, which is introduced for the first time here and will be defined below.

Fig. 2(b) shows the final block diagram of the network topology and direct-detection receiver. The input signal $E_s(t)$ and equivalent input ASE noise $n_{\mathrm{eq}}(t)$ are propagating through different channels which are represented by the transfer function $H_c(f)$ and the equivalent transmittance $T_{\mathrm{eq}}(f)$, respectively.

[1]This paper focuses exclusively on the impact of optical MUX/DMUX concatenation on the network performance. The interplay between bandwidth narrowing due to optical MUX/DMUX concatenation and fiber effects, which cause spectral broadening (e.g., self-phase modulation), is not considered here and will be addressed in future work.

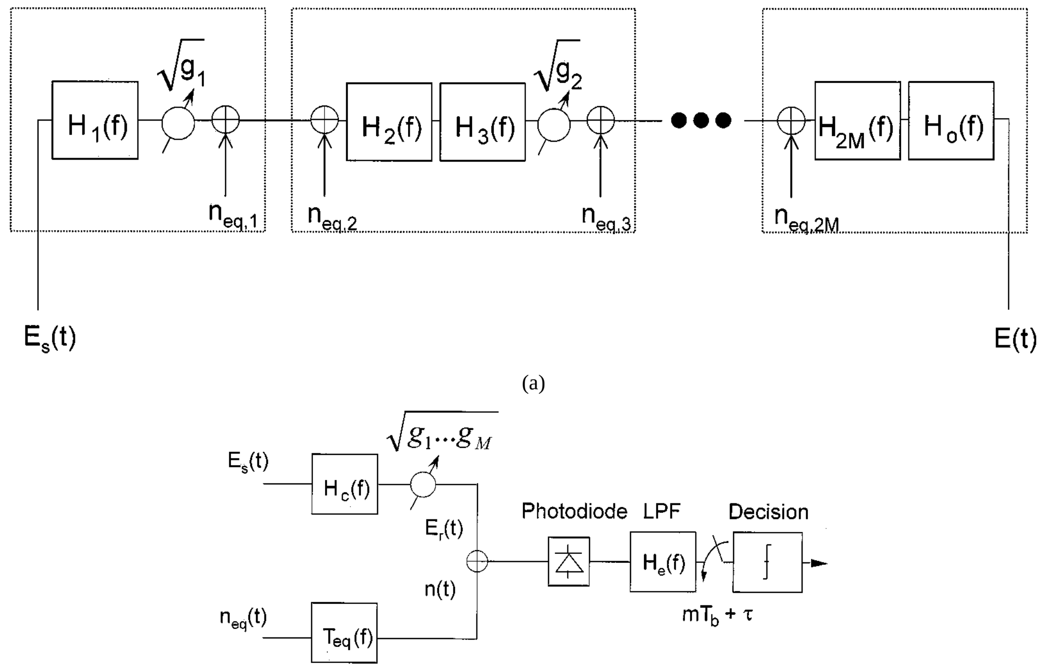

Fig. 2. (a) Simplified block diagram of the network topology shown in Fig. 1(a) ($E_s(t)$: input signal; g_i: ith attenuator gain; $n_{\mathrm{eq},i}(t)$: ith EDFA ASE noise). (b) Final block diagram of the network topology shown in Fig. 1(a) ($H_c(f)$ = transfer function of the signal channel; $T_{\mathrm{eq}}(f)$ = equivalent transmittance of the ASE noise channel; $n_{\mathrm{eq}}(t)$ = equivalent input ASE noise).

The equivalent input ASE noise $n_{\mathrm{eq}}(t)$ is defined here as a fictitious white Gaussian noise source that, if placed at the input of the network, will produce the same noise at the receiver input as the one provided by all the optical amplifiers in the network. The equivalent transmittance $T_{\mathrm{eq}}(f)$ can be expressed as a function of the last $2M-1$ optical MUXs/DMUXs transmittances and the gains of the last $M-1$ servo-controlled attenuators.

We will compare the performance of the actual network element chain with the performance of a reference network element chain, which is defined for the first time here as follows. All optical MUXs/DMUXs are replaced with perfectly aligned, ideal optical MUXs/DMUXs exhibiting rectangular amplitude transfer function, and linear or zero phase transfer function. The amplitude transfer functions have the same insertion loss at the center frequency and the same equivalent noise bandwidth B_o as the individual actual optical MUXs/DMUXs. In addition, it is assumed that the ideal optical MUXs/DMUXs do not introduce any ISI. Finally, it is assumed that there is a polarizer in front of the tunable optical BPF in the optically preamplified receiver aligned along the received signal polarization and that the receiver electronic LPF is an integrate and dump filter with impulse response duration equal to the bit period T_b.

It is well known [49] that an optimum direct-detection receiver is composed of a matched optical BPF and a wide-band electronic LPF. The reason for the adoption of a suboptimum reference network as a fair standard for comparison is that commercially available optical MUXs/DMUXs are designed in order to obtain maximally flat passband and minimum chromatic dispersion rather than matched filter characteristics. Nevertheless, the choice of reference network does not affect the essence of the results in Section III, but only the relative power penalties in Figs. 9–11.

B. Signal and Noise Representation

For mathematical convenience, a low-pass equivalent representation [49] of the optical signals and components is used in the following. To distinguish vectors from scalars, we identify vector quantities with boldface type. Matrices are also denoted by boldface type. The distinction should be clear from the context.

The electric field $\mathbf{E}_s(t)$ at the output of the transmitter can be written as $\mathbf{E}_s(t) = 2\sqrt{\bar{P}_s}\bar{E}_s(t)\hat{s}$, where $\bar{P}_s$ is the average signal power, $\hat{s}$ is the normalized Jones vector for the transmitted state of polarization, and $\bar{E}_s(t)$ is the normalized complex envelope that can be written as

$$\bar{E}_s(t) = s(t)e^{i\{2\pi[\Delta f + f_d(t)]t + \phi(t)\}} \tag{1}$$

where $s(t)$ is the amplitude of the normalized complex envelope $\bar{E}_s(t)$ (taking values in the range $[0,1]$), Δf is the offset of the transmitter's actual carrier frequency from the channel's nominal frequency f_s, $f_d(t)$ is the deviation of the transmitter's instantaneous frequency from the transmitter's actual carrier frequency $f_s + \Delta f$ (i.e., chirp), and $\phi(t)$ is the transmitter's phase noise.

The received electric field vector can be written as $\mathbf{E}_r(t) = 2\sqrt{\bar{P}_s}\bar{E}_r(t)\hat{r}$, where $\hat{r}$ is the normalized Jones vector for the received state of polarization, and $\bar{E}_r(t)$ is the normalized complex envelope of the received electric field that can be written as a function of the normalized complex envelope of the transmitted electric field

$$\bar{E}_r(t) = \sqrt{G_s}h_c(t) * \bar{E}_s(t) \tag{2}$$

where G_s is the signal effective gain provided by the reduction of the insertion loss of the M servo-controlled attenuators, specifically $G_s = g_1, \ldots, g_M$, $*$ denotes convolution, and $h_c(t)$ is the impulse response of the cascade of $2M$ optical MUXs/DMUXs and the receiver's tunable optical BPF

$$h_c(t) = \mathcal{F}^{-1}[H_c(f)] = \mathcal{F}^{-1}\left[\prod_{i=1}^{2M} H_i(f)H_o(f)\right] \quad (3)$$

where the operator $\mathcal{F}^{-1}$ denotes the inverse Fourier transform.

The ith attenuator gain g_i is equal to

$$g_i = \frac{\bar{P}_{\mathrm{in}}^{(i)}}{\bar{P}_{\mathrm{out}}^{(i)}} \quad (4)$$

where $\bar{P}_{\mathrm{in}}^{(i)}$ and $\bar{P}_{\mathrm{out}}^{(i)}$ denote the total average input/output powers to/from the optical MUX/DMUX pair of the ith node, respectively.

The received ASE noise is unpolarized and can be analyzed into two orthogonal states of polarization $\hat{r}$ and $\hat{p}$, parallel and perpendicular to the received signal's electric field, respectively

$$\mathbf{n}(t) = n_r\hat{r} + n_p\hat{p} \quad (5)$$

where n_r and n_p are independent identically distributed (i.i.d.) complex bandpass Gaussian processes with two-sided power spectral density (psd)

$$\Phi(f) = N_0 T_{\mathrm{eq}}(f) \quad (6)$$

where N_0 is the two-sided equivalent input ASE noise psd for each polarization and $T_{\mathrm{eq}}(f)$ is the transmittance of the equivalent channel seen by the equivalent input ASE noise. In the general case, the two EDFAs within each network element have different gains and noise figures. Assuming, without loss of generality, that all EDFAs are identical, that the spontaneous emission factor n_{sp} and the EDFA gain G are independent of frequency within the signal band, and that $G - 1 \simeq G$, N_0 can be written as

$$N_0 \simeq 2Mh(f_s + \Delta f)n_{\mathrm{sp}}G \quad (7)$$

where h is the Planck's constant.

In (6), $T_{\mathrm{eq}}(f)$ is calculated through the relationship

$$T_{\mathrm{eq}}(f) = \frac{1}{M}|H_o(f)|^2|H_{2M}(f)|^2 P_M(f) \quad (8)$$

where $P_n(f)$ is an auxiliary variable defined by the recursion

$$P_n(f) = 1 + g_n|H_{2n-1}(f)|^2|H_{2n-2}(f)|^2 P_{n-1}(f) \quad (9)$$

with initial condition $P_1(f) = 1$. The subscript n denotes the number of fiber spans.

Inspection of (8) reveals that $T_{\mathrm{eq}}(f)$ has gain due to the action of servo-controlled attenuators. We can rewrite $T_{\mathrm{eq}}(f)$ in the form $T_{\mathrm{eq}}(f) = FT_{\mathrm{eq},n}(f)$, where $T_{\mathrm{eq},n}(f)$ is normalized to unity and F is defined as the excess noise factor

$$F \triangleq T_{\mathrm{eq}}(0). \quad (10)$$

The variance of the orthogonally polarized components n_r, n_p of the ASE noise at the output of the chain of network elements can be calculated by integration of (6)

$$\sigma^2 = \int_{-\infty}^{\infty} \Phi(f)df = N_0 F B_{\mathrm{eq}} \quad (11)$$

where B_{eq} is the equivalent noise bandwidth of the chain of network elements defined as

$$B_{\mathrm{eq}} = \int_{-\infty}^{\infty} T_{\mathrm{eq},n}(f)df. \quad (12)$$

The total received electric field vector $\mathbf{E}(t)$ impingent upon the photodetector can be written as

$$\mathbf{E}(t) = \mathbf{E}_r(t) + \mathbf{n}(t) = \sigma\left\{[A\bar{E}_r(t) + \bar{n}_r(t)]\hat{r} + \bar{n}_p(t)\hat{p}\right\} \quad (13)$$

where $\bar{n}_r(t)$ and $\bar{n}_p$ are i.i.d. complex bandpass Gaussian processes with zero mean and unit variance and the multiplication coefficient A is written as

$$A = 2\frac{\sqrt{\bar{P}_s}}{\sigma} = 2\sqrt{\frac{\bar{E}_b}{N_0 F B_{\mathrm{eq},n}}} \quad (14)$$

where $\bar{E}_b = \bar{P}_s T_b$ denotes the average signal energy and $B_{\mathrm{eq},n} = B_{\mathrm{eq}} T_b$ denotes the normalized equivalent noise bandwidth. The quantity $\bar{E}_b/N_0$ represents the received optical signal-to-noise ratio (OSNR) measured in a resolution bandwidth equal to the bit rate.

Relationship (13) can be rewritten in terms of the quadrature components of the signal and ASE noise

$$\begin{aligned}\mathbf{E}(t) = \sigma&\left\{[A\bar{E}_{r_c}(t) + \bar{n}_{r_c}(t)] + i[A\bar{E}_{r_s}(t) + \bar{n}_{r_s}(t)]\right\}\hat{r}\\ &+\sigma[\bar{n}_{p_c}(t) + i\bar{n}_{p_s}(t)]\hat{p}\end{aligned} \quad (15)$$

where $\bar{E}_{r_c}(t)$, $\bar{n}_{r_c}(t)$ and $\bar{n}_{p_c}(t)$ are the real parts of the signal and ASE noise in the $\hat{r}$ and $\hat{p}$ polarizations, respectively, and $\bar{E}_{r_s}(t)$, $\bar{n}_{r_s}(t)$ and $\bar{n}_{p_s}(t)$ are the imaginary parts of the signal and ASE noise in the $\hat{r}$ and $\hat{p}$ polarizations, respectively.

The photodiode is modeled as a square law detector. The optical power measured by the photodetector is defined as

$$\begin{aligned}P(t) =& \frac{1}{2}||\mathbf{E}(t)||^2\\ =& \frac{\sigma^2}{2}\left\{A^2|\bar{E}_r(t)|^2 + 2A[\bar{E}_{r_c}(t)\bar{n}_{r_c}(t) + \bar{E}_{r_s}(t)\bar{n}_{r_s}(t)]\right.\\ &\left.+\bar{n}_{r_c}^2(t) + \bar{n}_{r_s}^2(t) + \bar{n}_{p_c}^2(t) + \bar{n}_{p_s}^2(t)\right\}.\end{aligned} \quad (16)$$

In the presence of a polarizer in front of the tunable optical BPF in the optically preamplified receiver aligned along the $\hat{r}$ polarization, the last two terms $\bar{n}_{p_c}^2(t)$ and $\bar{n}_{p_s}^2(t)$ on the right-hand side of (16) are omitted.

The final expression for the output photocurrent is

$$\begin{aligned}i_o(t) = \frac{R\sigma^2}{2}&[s_o(t) + n_{s\text{-ASE}}(t) + n_{\text{ASE–ASE}}(t)]\\ &+\sigma_s\bar{n}_s(t) + \sigma_t\bar{n}_t(t)\end{aligned} \quad (17)$$

where R is the responsivity of the photodiode, $s_o(t)$ is the term associated with the direct-detection of the signal, $n_{s\text{-ASE}}(t)$ denotes the signal-ASE noise beating, and $n_{\text{ASE–ASE}}(t)$ denotes the ASE–ASE noise beating in dimensionless form

$$\begin{aligned} s_o(t) &= A^2|\bar{E}_r(t)|^2 * h_e(t) \\ n_{s\text{-ASE}}(t) &= 2A[\bar{E}_{r_c}(t)\bar{n}_{r_c}(t) + \bar{E}_{r_s}(t)\bar{n}_{r_s}(t)] * h_e(t) \end{aligned} \tag{18}$$

$$n_{\text{ASE–ASE}}(t) = \left[\bar{n}^2_{r_c}(t) + \bar{n}^2_{r_s}(t) + \bar{n}^2_{p_c}(t) + \bar{n}^2_{p_s}(t)\right] * h_e(t). \tag{19}$$

In (17), $\bar{n}_s(t)$ and $\bar{n}_t(t)$ are i.i.d. real Gaussian processes with zero mean and unit variance that represent the shot and thermal noise, respectively.

In reality, shot noise follows Poisson statistics, e.g., [31], [33], [35], [36], [38], and [39]. Here, the shot-noise variance σ_s^2 is calculated approximately assuming that the level of the received signal $|\bar{E}_r(t)|$ is constant within the bit period with amplitude equal to $|\bar{E}_r(t_m)|$. If we neglect the dark current, the shot noise variance can be written as [50]

$$\sigma_s^2 = eR\sigma^2[A^2|\bar{E}_r(t_m)|^2 + 2p]B_e \tag{20}$$

where e is the electron charge, p is an auxiliary variable that takes the values $p = 1, 2$ in the presence or absence of polarizer, respectively, and B_e is the equivalent noise bandwidth of the electronic filter defined as [51]

$$B_e = \frac{1}{2}\int_{-\infty}^{\infty} |H_e(f)|^2 df. \tag{21}$$

The above expressions can be easily modified for avalanche photodiodes [50].

The thermal noise is a zero mean Gaussian noise with variance [50]

$$\sigma_t^2 = \frac{4KTF_eB_e}{R_L} \tag{22}$$

where K is the Boltzman's constant, T is the absolute temperature, F_e is the electronic preamplifier noise figure, and R_L is the load resistor.

C. Photocurrent Statistics

At the sampling instant $t_m = mT_b + \tau + \tau_\delta$, the value of the photocurrent at the output of the sampler is $i_o(t_m) = i_m$. For the evaluation of the error probability, it is necessary to calculate the statistics of the random variable (RV) i_m. This can be done through the characteristic function $\psi_{i_m}(v) = E\{e^{ivi_m}\}$, where $E\{.\}$ denotes the expected value.

The analytic evaluation of the characteristic function $\psi_{i_m}(v)$ can be done using the same formulation as in [26]–[41]. Our derivation is based on a generalization of the analysis by [37]. Our modifications of [37] allow to take into account arbitrary optical MUXs/DMUXs transfer functions, the polarizer at the receiver, and the shot noise (assuming Gaussian pdf), which are not included in [37].

As shown in the Appendix A, the characteristic function $\psi_{i_m}(v)$ of i_m is given by

$$\begin{aligned} \psi_{i_m}(v) &= E\left\{e^{ivi_m}\right\} \\ &= e^{\frac{ivR\sigma^2 s_o(t_m)}{2}} e^{-\frac{v^2\left(\sigma_t^2+\sigma_s^2\right)}{2}} \\ &\quad \times \prod_{k=1}^{\infty} \frac{e^{-\frac{v^2A^2R\sigma^2\left(b^2_{r_c,k}+b^2_{r_s,k}\right)}{1-2iva_k}}}{(1-2iva_k)^p} \end{aligned} \tag{23}$$

where the coefficients a_k, $b_{r_c,k}$, $b_{r_s,k}$, and $k = 1, \ldots$, are defined in Appendix A.

From the characteristic function, it is possible to evaluate the pdf of the photocurrent $p_{i_m}(i_m)$ by taking the Fourier transform of $\psi_{i_m}(v)$, i.e., $p_{i_m}(i_m) = \mathcal{F}[\psi_{i_m}(v)]$. In the general case, a closed-form analytic solution for $p_{i_m}(i_m)$ does not exist. The asymptotic value of $p_{i_m}(i_m)$ can be found using the steepest descent method [46]

$$p_{i_m}(i_m) \sim \frac{1}{\sqrt{2\pi[-f''(v_0)]}} e^{f(v_0)} \tag{24}$$

where the prime denotes differentiation with respect to v, v_0 is the root of the first derivative $f'(v_0) = 0$ and $f(v)$ is an auxiliary phase function defined as

$$f(v) = -ivi_m + \ln[\psi_{i_m}(v)]. \tag{25}$$

It is also commonplace to approximate $p_{i_m}(i_m)$ by a Gaussian pdf with mean μ_{i_m} and standard deviation σ_{i_m}. The mean μ_{i_m} and standard deviation σ_{i_m} can be evaluated from the characteristic function $\psi_{i_m}(v)$ using the relationship [49]

$$\mu_n = (-i)^n \left.\frac{d^n\psi_{i_m}(v)}{dv^n}\right|_{v=0} \tag{26}$$

where μ_n are the noncentral moments and $\mu_{i_m} = \mu_1$, $\sigma^2_{i_m} = \mu_2 - \mu_1^2$.

D. Error-Probability Evaluation

Finally, we use a semianalytic method [25] for the accurate evaluation of the error probability of the network. As its name indicates, the method consists of a combination of simulation and analysis. Noiseless simulation is used to evaluate the accumulation of ISI during signal propagation. Given the signal waveform at the receiver, the noise cdf and the error probability are calculated analytically.

The semianalytic method assumes that the ISI is caused primarily by a limited number Λ of bits. Here, it is assumed that the transmission channel is causal, so each bit is affected by the previous $\Lambda - 1$ bits. For example, consider that b_m is the bit that we want to detect and $\mathbf{b_m} = \{b_{-\Lambda+m+1}, \ldots, b_m\}$ is a sequence of the Λ last received bits. Then, the mean error probability $\bar{P}_e$ can be calculated by averaging over all the 2^Λ possible combinations of Λ bits

$$\bar{P}_e = \sum_{m=1}^{2^\Lambda} p_{\mathbf{b_m}}(\mathbf{b_m}) P_e(\bar{b}_m|\mathbf{b_m}) \tag{27}$$

where $p_{\mathbf{b_m}}(\mathbf{b_m})$ is the probability of occurrence of the combination of bits $\mathbf{b_m}$ and $P_e(\bar{b}_m|\mathbf{b_m})$ is the conditional probability to receive the complementary symbol $\bar{b}_m$, given that the particular combination of bits $\mathbf{b_m}$ was sent.

The conditional error probability $P_e(\bar{b}_m|\mathbf{b_m})$ is defined as follows:

$$P_e(\bar{b}_m|\mathbf{b_m}) = \begin{cases} \int_D^{\infty} p_{i_m}(i_m)di_m, & b_m = 0 \\ \int_{-\infty}^{D} p_{i_m}(i_m)di_m, & b_m = 1 \end{cases} \quad (28)$$

where D is the decision threshold. The optimum value of the decision threshold D, which minimizes the mean error probability $\bar{P}_e$, is the root of the first derivative of (27) with respect to D. The integrals (28) must be evaluated numerically.

An alternative expression for the conditional error probability $P_e(\bar{b}_m|\mathbf{b_m})$ can be found by substitution of $p_{i_m}(i_m) = \mathcal{F}[\psi_{i_m}(v)]$ in (28)

$$P_e(\bar{b}_m|\mathbf{b_m}) = \begin{cases} \frac{1}{2\pi}\int_{-\infty}^{\infty} \frac{\psi_{i_m}(v)}{iv} e^{-ivD}dv, & b_m = 0 \\ -\frac{1}{2\pi}\int_{-\infty}^{\infty} \frac{\psi_{i_m}(v)}{iv} e^{-ivD}dv, & b_m = 1 \end{cases} \quad (29)$$

The asymptotic value of the integrals in (29) can be found using, again, the steepest descent method [26], [38], [41], [46].

If we approximate $p_{i_m}(i_m)$ by a Gaussian pdf with mean μ_{i_m} and standard deviation σ_{i_m}, substitution in (28) gives

$$P_e(\bar{b}_m|\mathbf{b_m}) = \begin{cases} \frac{1}{2}\mathrm{erfc}\left(\frac{D-\mu_{i_m}}{\sqrt{2}\sigma_{i_m}}\right), & b_m = 0 \\ \frac{1}{2}\mathrm{erfc}\left(\frac{\mu_{i_m}-D}{\sqrt{2}\sigma_{i_m}}\right), & b_m = 1 \end{cases} \quad (30)$$

where erfc(.) is the complementary error function [52] defined as $\mathrm{erfc}(x) = 2/\sqrt{\pi}\int_x^{\infty} e^{-t^2}dt$.

E. Error Probability for the Reference Network

For the reference network, the mean error probability is approximately given by [31]

$$\bar{P}_e = \frac{1}{2}\left[1 + e^{-\frac{2d\bar{E}_b}{N_0}} \sum_{k=0}^{M_0-1} \frac{1}{k!}\left(\frac{2\bar{E}_b}{N_0}\right)^k - Q_{M_0}\left(2\sqrt{\frac{\bar{E}_b}{N_0}}, 2\sqrt{\frac{d\bar{E}_b}{N_0}}\right)\right] \quad (31)$$

where M_0 is an integer number, approximately equal to the bit period-optical bandwidth product, i.e., $M_0 = \lceil B_o T_b \rceil$, $\lceil x \rceil$ denotes the least integer not smaller than x, d is the normalized optimum threshold defined in the interval $[0, 1]$, and $Q_{M_0}(\alpha, \beta)$ is the generalized Marcum function [49] defined by

$$Q_n(\alpha, \beta) = \int_b^{\infty} x\left(\frac{x}{\alpha}\right)^{n-1} \times \exp\left[-\frac{1}{2}(x^2+\alpha^2)\right] I_{n-1}(\alpha x)dx \quad (32)$$

where $I_n(.)$ denotes the modified Bessel function of the first kind of order n.

For $M_0 = 1$, (31) becomes identical to the error probability of a matched filter direct-detection receiver.

III. Study Case—Concatenation of AWG Routers

AWG routers are a promising technology for transparent dense wavelength-division multiplexing networks due to their ability to multiplex/demultiplex a large number of channels, their negligible chromatic dispersion, their compactness (i.e., integrated form) and their low cost [53]. Disadvantages of conventional AWG routers are the relatively high insertion loss and the passband curvature [54]. Several techniques to increase the passband flatness are proposed in the literature. However, there is a tradeoff between passband flatness and insertion loss [54].

This section presents an accurate study of the concatenation of conventional AWG routers (i.e., with round passband top) in a transparent multiwavelength optical network chain like the one presented in Fig. 1(a). This subject was partly studied previously by [6] and [11] for 10-Gb/s nonreturn-to-zero (NRZ) and by [17] for 40 Gb/s return-to-zero (RZ) transmission. The main purpose of this study case is to illustrate the theoretical model of Section II.

This section is divided into two parts. In the first part, we examine whether a Gaussian function can describe well the top of the transmittance of commercially available conventional AWG routers. In addition, we investigate the importance of random central frequency offsets from the channels' nominal frequencies and the variations of the 3-dB filter bandwidth from channel to channel and from device to device.

The second part is devoted to the evaluation of the error probability of a chain network with AWG routers as a function of the number of fiber spans, the equivalent noise bandwidth of AWG routers, and the laser carrier frequency offset from the channel's nominal frequency.

A. Transmittance of AWG Routers

Fig. 3 shows the measured transmittance from an input port to all output ports of a commercially available 8×8 conventional AWG router, with channels spaced 100-GHz apart. Dotted lines indicate the periodic transmittance of one of the channels. It is observed that the transmittance for each channel presents round top in the passband and side lobes in the stopband. In addition, it is observed that there is a systematic insertion loss difference between channels (loss imbalance [55]), i.e., edge channels within the free spectral range of the device exhibit more loss than the middle channel.

In equivalent low-pass formulation, the magnitude $|H_{\mathrm{AWG}}(f)|$ of the transfer function of each channel can be approximated at the center of the passband by a Gaussian function (see, e.g., [56])

$$|H_{\mathrm{AWG}}(f)| = \alpha e^{-1/2(f-f_0/f_c)^2} \quad (33)$$

where α is the insertion loss, f_0 is the central frequency offset from the channel's nominal frequency f_s, and f_c is the cutoff frequency, which is related to the 3-dB bandwidth (full-width at half-maximum) of the transmittance through

$$B_{3\ \mathrm{dB}} = 2\sqrt{\ln 2} f_c. \quad (34)$$

More relationships about the properties of this type of AWG router are given in Appendix B.

Obviously, the Gaussian approximation (33) does not describe the side lobes in the stopband (see Fig. 3). However, this discrepancy becomes less important as the number of concatenated optical MUXs/DMUXs increases. For example, accurate description of the transmittance of an individual

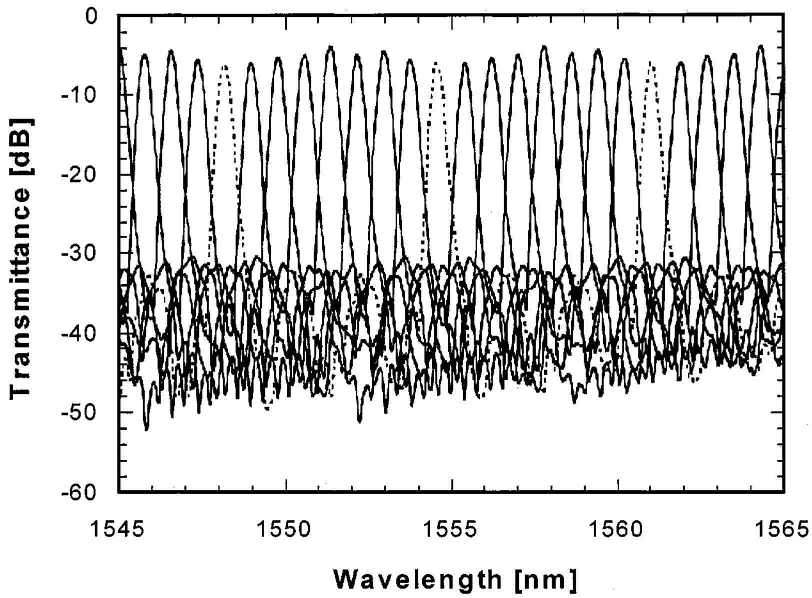

Fig. 3. Transmittance of a commercially available 8 × 8 AWG router with channels spaced 100-GHz apart from an input port to all eight output ports. Dotted lines indicate the periodic transmittance of one of the channels.

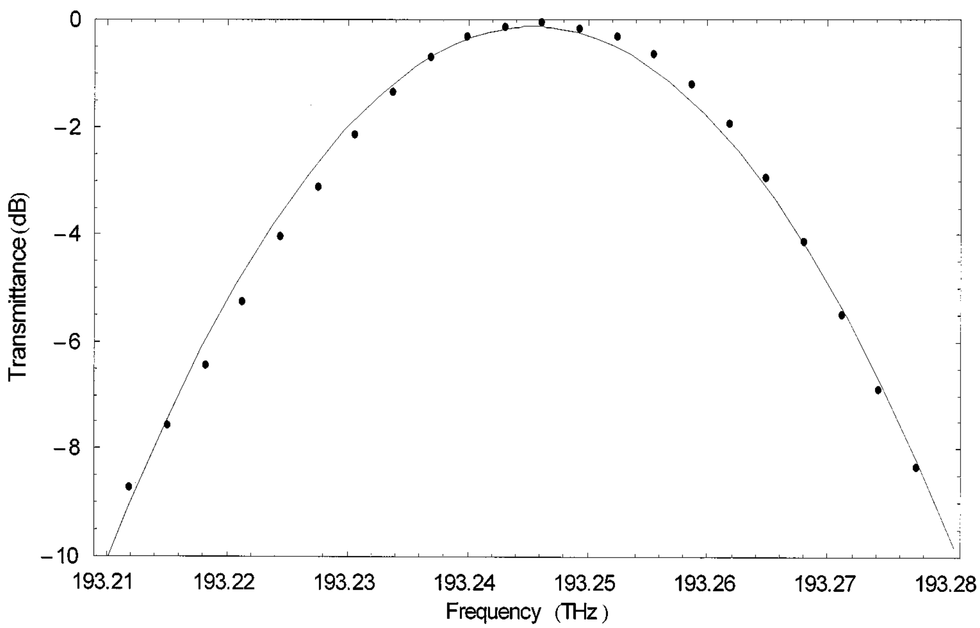

Fig. 4. Measurements of the normalized transmittance of a sample AWG router channel from Fig. 3 (points) and their fitting by the square of (33) (solid line).

optical MUX or DMUX within only 10 dB from the top of the passband is sufficient for the description of the overall transfer function of a chain of ten optical MUXs/DMUXs within 100 dB from the top of the passband.

In addition, in (33), it is assumed that the optical AWG routers are not dispersive devices within the signal band and the phase is set equal to zero. In practice, small variations of refractive indixes, width, and thickness from waveguide to waveguide induce amplitude and phase errors in the transfer function. Nevertheless, these errors are assumed small and the behavior of the device is dominated by the curvature of the passband [21], [57], [58].

Fig. 4 shows measurements of the normalized transmittance of one AWG router channel from Fig. 3 (points) and their fitting by the square of (33) (solid line). Measurements within 10 dB from the top of the passband are used for the fitting; the fit is excellent. We conclude that the Gaussian approximation accurately describes the behavior of the transmittance of conventional AWG routers in the center of the passband and its vicinity.

Fitting of the normalized transmittance measurements is used next for the extraction of the center frequency and the 3-dB bandwidth and the evaluation of their statistics.[2] For this purpose, measurements of the transmittance of two commer-

[2]It is worth noting that there is no universally accepted method for the measurement of the center frequency and the 3-dB bandwidth of optical MUXs/DMUXs. For example, commercially available devices are often characterized by measuring the 3-dB points from the top of the passband and defining their average as the center frequency.

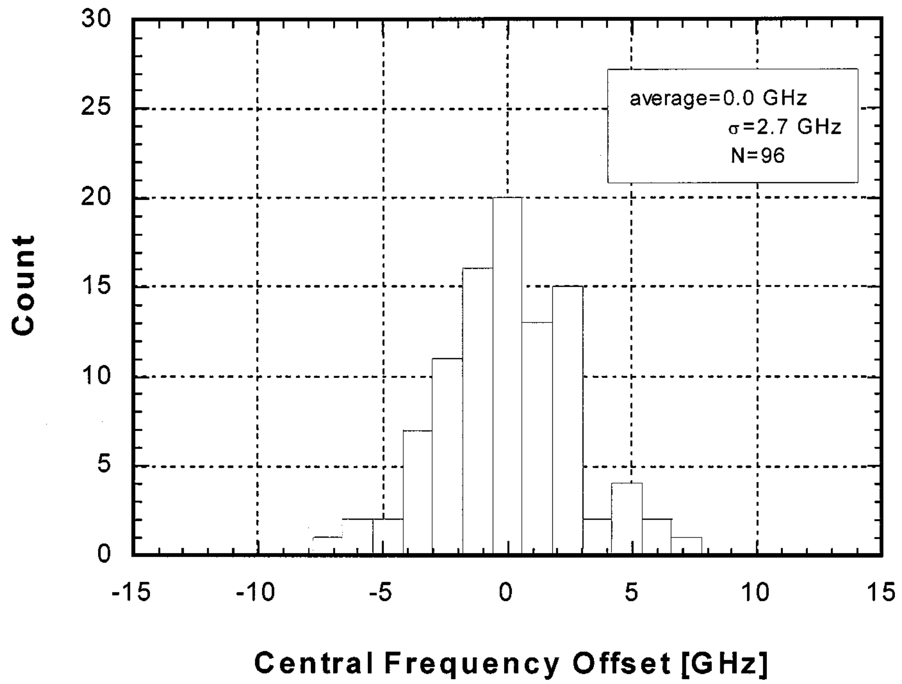

Fig. 5. Histogram of AWG router central frequency offsets from the channels' nominal frequencies (based on measurements of 96 transmittances).

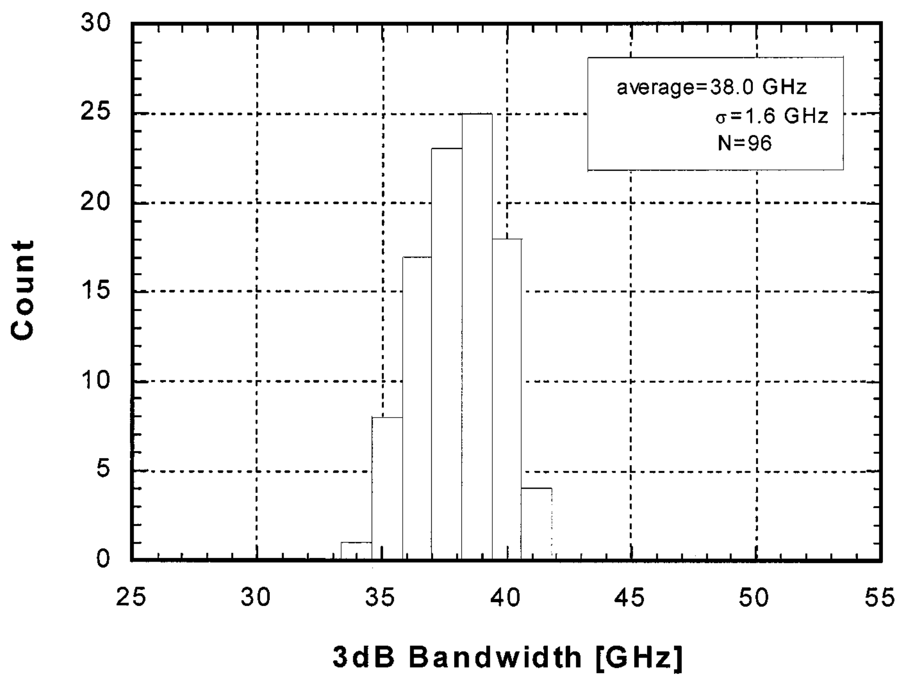

Fig. 6. Histogram of 3-dB bandwidths of AWG router channels (based on measurements of 96 transmittances).

cially available 8×8 conventional AWG routers, with channels spaced 100-GHz apart, are fitted by the square of (33). Due to the lack of a large sample of devices, we made the (arbitrary) assumption that the transfer functions of different channels and different input/output ports within the same device are independent. This assumption is not strictly correct so the extracted center frequencies and 3-dB bandwidths are partly correlated. In addition, as a result of our assumption, we make no distinction between random and systematic error. Consequently, the following statistics provide only a rough estimation of the importance of random variations in the transmittance of AWG routers.

Histograms for the central frequency offsets from the channels' nominal frequencies and the 3-dB bandwidths for two commercially available 8×8 conventional AWG routers, with channels spaced 100-GHz apart, are presented in Figs. 5 and 6, respectively. Fig. 5 shows that central frequency offsets from the channels' nominal frequencies are concentrated around zero in a range (-8 GHz, $+8$ GHz), with standard deviation of 2.7 GHz, which is about 7% of the mean 3-dB filter bandwidth. Fig. 6

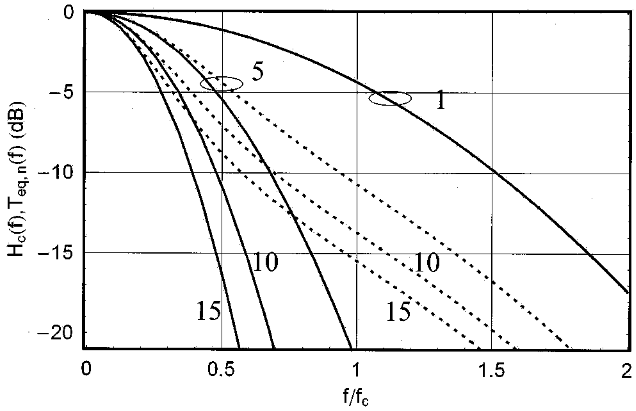

Fig. 7. Signal transfer function $H_c(f)$ (solid lines) and normalized transmittance $T_{\mathrm{eq},n}(f)$ (dotted lines) of the chain of network elements seen by the equivalent input ASE noise for one, five, ten, and 15 fiber spans.

shows that the mean 3-dB bandwidth is 38 GHz, with a standard deviation of 1.6 GHz, which is 4% of the mean 3-dB filter bandwidth.

Based on the above, we conclude that the random central frequency offsets from the channels' nominal frequencies and the variations of the 3-dB filter bandwidth of commercially available AWG routers are small and, in a first approximation, can be neglected. In the following, the transfer functions of concatenated AWG routers will be considered identical and perfectly aligned. The impact of random variations on the system's performance will be addressed in a future paper.

B. AWG Router Cascadability

The AWG router cascadability depends on the selection of network design parameters, e.g., transmitted optical pulse shape, extinction ratio, chirp, fiber chromatic dispersion and nonlinearities, receiver type, and so forth. An exhaustive study of the influence of all possible combinations of the aforementioned parameters on the network performance is beyond the scope of this example. To isolate the impact of the AWG router filtering from other transmission effects, the following network parameter set is used in this study: ideal NRZ pulses with infinite extinction ratio and zero chirp, absence of chromatic dispersion and nonlinearities, ASE-noise-limited direct-detection receiver, negligible shot and thermal noises, and a fourth-order Bessel electronic LPF with cutoff frequency $0.7R_b$ (i.e., equivalent noise bandwidth $B_e = 0.73R_b$).

Appendix C presents the details of the implementation of the semianalytic method for the error-probability evaluation in this specific case study.

Fig. 7 shows the signal transfer function $H_c(f)$ (solid lines) and the normalized transmittance $T_{\mathrm{eq},n}(f)$ seen by the equivalent input ASE noise (dotted lines) for one, five, ten, and 15 fiber spans. Since all curves present symmetry around the origin, only the positive frequency semiaxis is displayed. It is observed from (6) that $T_{\mathrm{eq},n}(f)$ depends on the effective attenuator gains g_i, $2, \ldots, M$. Here, we assumed that all attenuator gains g_i, $2, \ldots, M$ are unity (case of wide AWG routers compared to the signal spectral occupancy). It is observed that $H_c(f)$ and $T_{\mathrm{eq},n}(f)$ coincide in the proximity of the origin for any number of fiber spans. Away from the origin, they are very different for $M \neq 1$ and their discrepancy increases as a function of the number of spans. At the limit $f \gg f_c, T_{\mathrm{eq},n}(f) \to |H(f)|^2/M$. The behavior of $T_{\mathrm{eq},n}(f)$ implies that the filtering of the ASE noise by the optical MUX/DMUX chain is less severe than the filtering of the signal due to the distributed generation of the ASE noise in the network. We conclude that, for a large number of fiber spans, it is beneficial to use a narrow-band optical BPF at the optically preamplified direct-detection receiver for rejection of the long ASE noise tails.

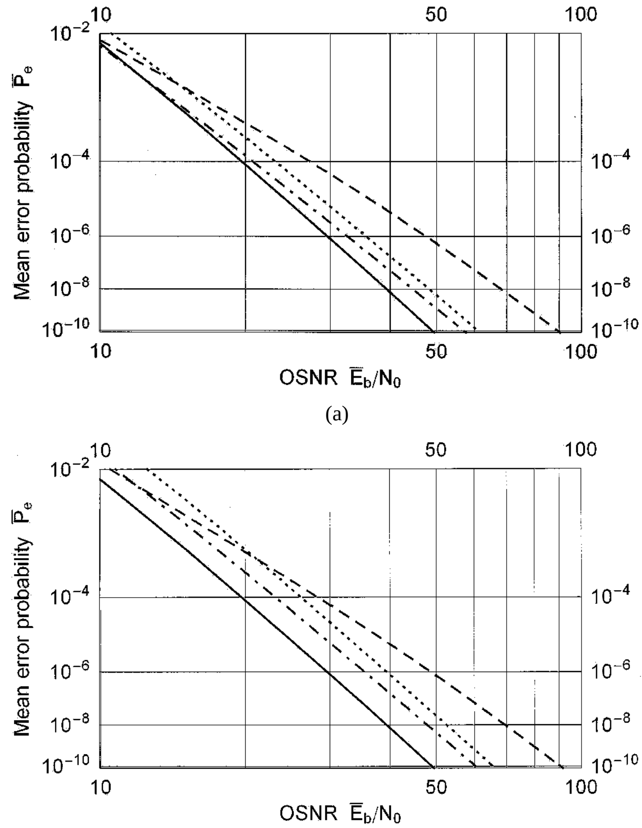

(a)

(b)

Fig. 8. Mean error probability $\bar{P}_e$ as a function of the received OSNR $\bar{E}_b/N_0$ measured in a resolution bandwidth equal to the bit rate for one (dotted line), three (dashed-dot line), and 12 (dashed line) fiber spans. (a) In the presence of polarizer at the receiver. (b) In the absence of polarizer at the receiver (condition: $B_o = 4R_b$).

Fig. 8(a) and (b) shows the mean error probability $\bar{P}_e$ as a function of the received OSNR $\bar{E}_b/N_0$ measured in a resolution bandwidth equal to the bit rate for one (dotted line), three (dashed-dot line), and 12 (dashed line) fiber spans, in the presence and in the absence of polarizer at the receiver respectively. The equivalent noise bandwidth of individual AWG routers in these graphs is assumed $B_o = 4R_b$. (For example, in the case of the AWG routers shown in Fig. 3, which exhibit a mean equivalent noise bandwidth equal to 40.5 GHz, the above assumption implies a bit rate $R_b \simeq 10$ Gb/s.) For a comparison, the error probability for the reference network (31) is also shown (solid line). In Fig. 8(a), for one fiber span, 1.4 dB of additional power compared to the reference network are required to achieve an error probability of 10^{-9}. When the number of spans increases, initially the sensitivity is improved because

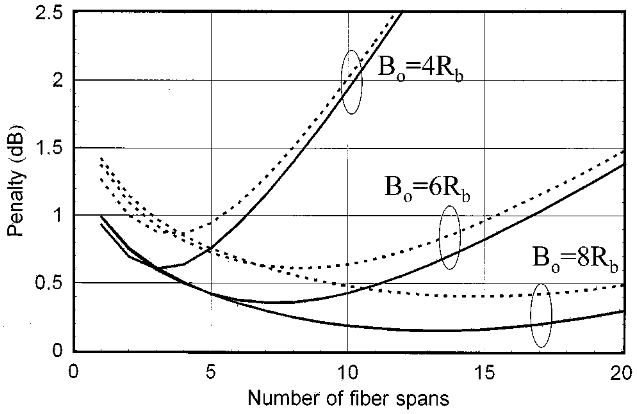

Fig. 9. Optical power penalty compared to the reference network, at an error probability of 10^{-9}, as a function of the number of fiber spans, for three individual AWG router equivalent noise bandwidths, i.e., $B_o = 4R_b$, $6R_b$, and $8R_b$, in the presence (solid lines) or absence (dotted lines) of polarizer, respectively.

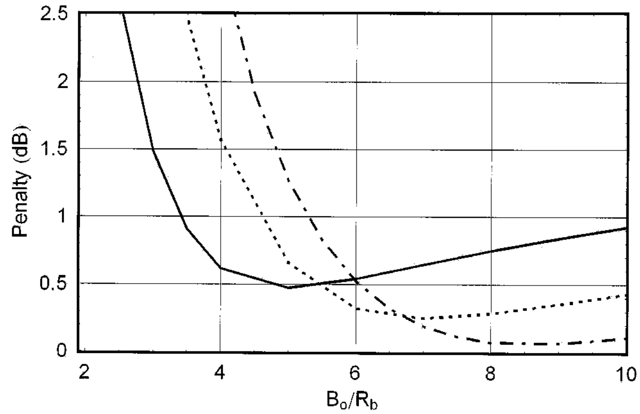

Fig. 10. Optical power penalty compared to the reference network, at an error probability of 10^{-9}, as a function of the equivalent noise bandwidth of the individual AWG routers for five (solid line), ten (dotted line), and 15 (dashed-dot line) fiber spans in the presence of polarizer at the receiver.

the optical bandwidth narrowing reduces the power of the ASE noise without essentially distorting the signal. A maximum sensitivity is achieved after three fiber spans, where there is only 0.61 dB power penalty compared to the reference network. As the number of spans continues to increase, the power penalty slowly increases due to the increase of ISI. It is observed that the slope of the error-probability curves changes as a function of the number of fiber spans. This is due to the fact that AWG filtering changes the properties of the ASE noise at the input of the direct-detection receiver. Similar conclusions can be drawn from Fig. 8(b). Notice that, in Fig. 8(a), at high error probabilities (i.e., low OSNRs), the actual network for three fiber spans performs slightly better than the reference network. This apparent paradox is due to the fact that the reference network is suboptimum. A matched filter direct-detection receiver [not depicted in Fig. 8(a) and (b) to avoid clutter] presents superior performance than both the actual and the reference network at all error probabilities. For a matched filter direct-detection receiver, the OSNR measured in a resolution bandwidth equal to the bit rate required to achieve an error probability of 10^{-9} is approximately 38.5 (15.85 dB).

Fig. 9 shows the optical power penalty compared to the reference network at an error probability of 10^{-9} as a function of the number of fiber spans for three individual AWG router equivalent noise bandwidths, i.e., $B_o = 4R_b$, $6R_b$, and $8R_b$, in the presence (solid lines) or absence (dotted lines) of polarizer at the receiver. In the $B_o = 4R_b$ case, in the presence of polarizer, a minimum power penalty 0.61 dB is achieved after three fiber spans. In the absence of polarizer, a broad maximum sensitivity is achieved after four fiber spans, where there is only 0.87-dB power penalty compared to the reference network. In the $B_o = 8R_b$ case, in the presence of polarizer, a broad maximum sensitivity is achieved after 12 fiber spans, where there is only 0.16-dB power penalty compared to the reference network. In the absence of polarizer, a broad maximum sensitivity is achieved after fifteen fiber spans, where there is only 0.41-dB power penalty compared to the reference network. The results for the $B_o = 6R_b$ case fall in between the $B_o = 4R_b$ and $B_o = 8R_b$ cases. These results indicate that it is possible to concatenate an arbitrary number of conventional AWG routers, despite the inherent passband curvature of these devices, by increasing the equivalent noise bandwidth of individual AWG routers for fixed bit rate at the expense of channel spacing. In addition, it is observed that an ideal polarizer always improves the performance of the optically preamplified receiver, as expected, due to the elimination of the ASE–ASE noise beating terms $\bar{n}_{p_c}^2(t)$ and $\bar{n}_{p_s}^2(t)$ on the right-hand side of (16). The role of the polarizer is more important for larger individual AWG router equivalent noise bandwidths and smaller number of fiber spans. However, in all cases examined in the present paper, the performance improvement due to the polarizer is marginal (less than 0.5 dB) and does not justify the implementation cost of this device.

Using the current model, it is possible, in principle, to maximize the network performance for a given number of concatenated AWG routers by jointly optimizing the optical bandwidth of the individual AWG routers and the electronic LPF bandwidth of the receiver. However, such optimization is impractical because in transparent optical networks, each optical signal passes through a different number of concatenated AWG routers. In addition, in reconfigurable optical networks, each optical signal may be rerouted through several different paths during the network's lifetime, depending on traffic demands, equipment failures, and so forth. Nevertheless, it is instructive to examine the impact of the equivalent noise bandwidth of individual AWG routers on the performance of the network.

Fig. 10 shows the optical power penalty at an error probability of 10^{-9} (compared to the corresponding reference network at the optimum operating point) as a function of the equivalent noise bandwidth of individual AWG routers for constant electronic LPF equivalent noise bandwidth $0.73R_b$. We consider three different paths in the network, where the signal passes through five (solid line), ten (dotted line), and 15 (dashed-dot line) fiber spans in the presence of polarizer at the receiver. For five fiber spans, a minimum sensitivity is achieved at $B_o = 5R_b$, where there is only 0.47-dB power penalty compared to the corresponding reference network, which requires an OSNR of 16.6 dB at an error probability of 10^{-9}. In the case of ten fiber spans,

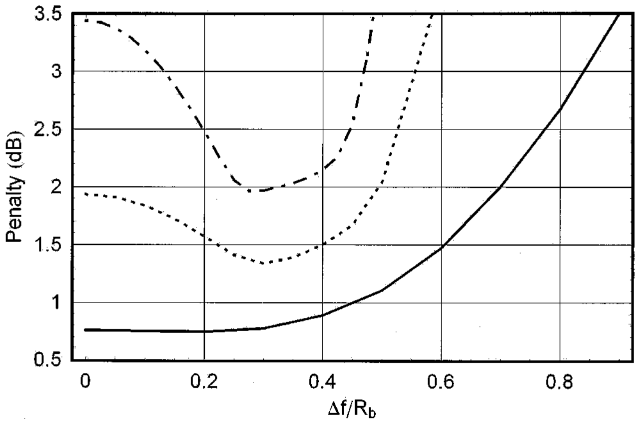

Fig. 11. Optical power penalty compared to the reference network, at an error probability of 10^{-9}, as a function of the laser carrier frequency misalignment from the channel's nominal frequency, when the signal passes through five (solid line), ten (dotted line), and 15 (dashed-dot line) fiber spans in the presence of polarizer at the receiver (condition: $B_o = 4R_b$).

a minimum sensitivity is achieved at $B_o = 7R_b$, where there is only 0.25-dB power penalty compared to the corresponding reference network, which requires an OSNR of 16.9 dB at an error probability of 10^{-9}. In the case of 15 fiber spans, a minimum sensitivity is achieved at $B_o = 9R_b$, where there is only 0.06-dB power penalty compared to the corresponding reference network, which requires an OSNR of 17 dB at an error probability of 10^{-9}. The sensitivity degrades sharply for narrower equivalent noise bandwidths. We conclude that a possible compromise is to choose the AWG router equivalent noise bandwidth equal to $B_o = 6R_b$, which guarantees an optical power penalty less than 0.5 dB in all cases.

Fig. 11 shows the optical power penalty compared to the reference network, at an error probability of 10^{-9}, as a function of the laser carrier frequency offset from the channel's nominal frequency when the signal passes through five (solid line), ten (dotted line), and 15 (dashed-dot line) fiber spans in the presence of polarizer at the receiver. Due to the symmetry in the optical signal spectrum and the AWG transfer function, the power penalty is the same for laser misalignments of the same magnitude, but different signs. Therefore, only the optical power penalty for positive misalignments is displayed. In the case of five fiber spans, the model predicts a monotonic increase in the optical power penalty as the laser carrier frequency offset increases. However, in the case of ten and 15 fiber spans, the model predicts a minimum optical power penalty of 1.34 and 1.97 dB, respectively, compared to the reference network for a laser carrier frequency offset $0.3R_b$ and $0.28R_b$, respectively, from the channel's nominal frequency. This surprising result, which occurs when the effective equivalent bandwidth of optical MUXs/DMUXs cascade becomes comparable to the bit rate, was first observed theoretically and experimentally by [6] and was attributed to the filtering of the vestigial side band. Preliminary simulations performed by the authors indicate that this effect is universal and can be observed for other modulation formats and optical MUXs/DMUXs types as well, e.g., Gaussian RZ pulses and MUXs/DMUXs composed of MI filters. Recently, this effect was proposed as a means to achieve ultrahigh-capacity WDM transmission [59] and was used to obtain record spectral efficiency 1.28 b/s/Hz in a 10.2-Tb/s transmission experiment [60].

IV. Summary

This paper presents a general theoretical model for the study of concatenation of optical MUXs/DMUXs in transparent multiwavelength optical networks. The model is based on a semianalytical technique [25] for the evaluation of the error probability. Approximate calculations of the error probability with semianalytical techniques, as a criterion for the cascadability of optical MUXs/DMUXs, were used in the past, e.g., [3] and [6]. However, the present technique offers superior accuracy, taking into account arbitrary pulse shapes, arbitrary optical MUX/DMUX and electronic LPF transfer functions, and non-Gaussian photocurrent statistics at the output of the direct-detection receiver assuming ideal square-law detection [26]–[41]. The computation of the error probability involves several steps, including expansion of the ASE noise impingent upon the photodiode in Karhunen–Loève series [42]–[44], numerical solution of the associated homogeneous Fredholm equation of the second kind [44]–[46], diagonalization of a quadratic form [37], [45], and asymptotic evaluation of the pdf at the output of the direct-detection receiver from the characteristic function using the method of steepest descent [26], [41], [46].

The model helps to identify the underlying mechanisms for performance degradation and to provide a rigorous definition for the excess loss due to spectral clipping resulting from optical MUX/DMUX concatenation. In addition, for the first time, the notions of effective gain and excess noise factor due to servo-controlled attenuators are introduced. Finally, a reference network with ideal optical MUXs/DMUXs is defined for comparison.

The model can be used to derive specifications for arbitrary optical MUXs/DMUXs in order to achieve a prescribed power penalty in conjunction with different modulation formats. To illustrate the model, the concatenation of conventional AWG routers in a transparent multiwavelength optical network chain is studied. First, measurements of the transmittance of commercially available AWG routers are fitted in order to extract the values of the channels' central frequencies and 3-dB bandwidths and evaluate their statistics. Statistical results indicate that first-order random variations in the transfer functions of AWG routers from device-to-device can be neglected. Then, the error probability is evaluated as a function of the number of AWG routers, the bandwidth of AWG routers, and the laser carrier frequency offset from the channel's nominal frequency.

Appendix A

Derivation of the Characteristic Function of the Output Photocurrent

The analytical evaluation of the characteristic function of the filtered noise at the output of a square-law detector was performed initially in the context of radio communications (e.g., see [26] and the references therein) and later in the context of optically preamplified direct-detection receivers, e.g., [27]–[41] for different types of optical and electronic LPFs.

Here, we adapt the formalism of [37] to the study of optical MUX/DMUX concatenation. For the sake of completeness, the derivation of the expression (23) for the characteristic function $\psi_{i_m}(v)$ is described briefly. The interested reader can find more details in [37]. Wherever possible, the same notation as in [37] is used. Our modifications of [37] consist of the inclusion of arbitrary optical MUXs/DMUXs transfer functions, the polarizer at the receiver, and the shot noise variance, borrowing elements from [27]–[41].

The derivation is divided into the following parts. In the first part, the convolutions in (18) and (19) describing the low-pass filtering of the signal–ASE and ASE–ASE noise beatings are transformed into sums of i.i.d. Gaussian RVs using a Karhunen–Loève expansion of the equivalent input ASE noise. In the second part, the characteristic function of the signal–ASE and ASE–ASE noise beatings is calculated. Finally, the shot and thermal contribution are added to the characteristic function.

As a starting point, we rewrite the photocurrent given in (17) at the output of the sampler

$$i_o(t_m) = \frac{R\sigma^2}{2}[s_o(t_m) + n_{s\text{-ASE}}(t_m) + n_{\text{ASE–ASE}}(t_m)] + \sigma_s\bar{n}_s(t_m) + \sigma_t\bar{n}_t(t_m) \quad (35)$$

where

$$\begin{aligned} s_o(t) &= A^2|\bar{E}_r(t)|^2 * h_e(t) \\ n_{s\text{-ASE}}(t) &= 2A[\bar{E}_{r_c}(t)\bar{n}_{r_c}(t) + \bar{E}_{r_s}(t)\bar{n}_{r_s}(t)] * h_e(t) \end{aligned} \quad (36)$$

$$n_{\text{ASE–ASE}}(t) = \left[\bar{n}^2_{r_c}(t) + \bar{n}^2_{r_s}(t) + \bar{n}^2_{p_c}(t) + \bar{n}^2_{p_s}(t)\right] * h_e(t). \quad (37)$$

For the evaluation of the statistics of (37), the equivalent input ASE noise quadrature components $\bar{n}_l(t),\ l = r_c, r_s, p_c, p_s$ are represented in the time interval $[0, \tau_e]$, where τ_e is the duration of the impulse response of the electronic LPF, by a Karhunen–Loève expansion [42], [43]

$$\bar{n}_l(t) = \sum_{k=1}^{\infty} c_{l,k}\phi_k(t) \quad (38)$$

where the coefficients $c_{l,k}$ are independent Gaussian RVs with zero mean and variance $\sigma^2_{l,k}$[42]–[44]. The orthonormal functions $\phi_k(t)$ and the variances $\sigma^2_{l,k}$ of $c_{l,k}$ are the eigenfunctions and the eigenvalues, respectively, of the homogeneous Fredholm equation of the second kind [45]

$$\int_0^{\tau_e} R_{\bar{n}_l}(t-t')\phi_k(t')dt' = \sigma^2_{l,k}\phi_k(t) \qquad l = r_c,\ r_s,\ p_c,\ p_s \quad t \in [0, \tau_e] \quad (39)$$

where $R_{\bar{n}_l}(t-t')$ is the autocorrelation function of $\bar{n}_l$ and can be evaluated by the real part of the inverse Fourier transform of $T_{\text{eq},n}(f)/B_{\text{eq}}$, i.e., $R_{\bar{n}_l}(\tau) = \Re\{\mathcal{F}^{-1}[T_{\text{eq},n}(f)/B_{\text{eq}}]\}$.

It is worth noting that the eigenfunctions and the eigenvalues for the real and imaginary parts of the $\hat{r}$ and $\hat{p}$ polarizations are always degenerate, i.e., $\sigma_{r_c,k} = \sigma_{r_s,k} = \sigma_{p_c,k} = \sigma_{p_s,k} = \sigma_k$, $\forall\, k$. However, if $T_{\text{eq},n}(f)$ does not present Hermitian symmetry around the origin, e.g., due to optical MUX/DMUX center frequency offsets or systematic passband tilts, then the real and imaginary parts of the ASE noise along the $\hat{r}$ and $\hat{p}$ polarizations and the corresponding coefficients $c_{l,k},\ l = r_c,\ r_s,\ p_c,\ p_s$ are cross correlated [49, pp. 153–157]. In the following, it is assumed that $T_{\text{eq},n}(f)$ presents Hermitian symmetry, as is the case for perfectly aligned AWG routers with symmetric transfer functions, so this cross correlation is negligible, i.e., $\Im\{\mathcal{F}^{-1}[T_{\text{eq},n}(f)/B_{\text{eq}}]\} = 0$, where $\Im$ denotes imaginary part.

Equation (39) can be solved analytically only in certain special cases of $R_{\bar{n}_l}(t-t')$ [44]. In the case of arbitrary optical MUX/DMUX transfer functions, (39) must be resolved numerically [46]. The method consists in using a quadrature rule for the integral in the left-hand side of (39) and in discretizing the time at the same nodes in order to create a matrix eigenvalue equation. For the quadrature, we use the trapezoidal rule because it allows for equally spaced nodes t_i and is, therefore, well suited for the evaluation of integrals (44), involving the signal $\bar{E}_r(t)$ provided from digital simulation.

Substituting the Karhunen–Loève expansion of $\bar{n}_l(t)$ into (37) yields

$$n_{l,\text{ASE–ASE}} = \sum_{k=1}^{\infty}\sum_{j=1}^{\infty} c_{l,k}c_{l,j}\Phi_{kj} \quad l = r_c,\ r_s,\ p_c,\ p_s \quad (40)$$

where we defined $\Phi_{kj} = \int_{-\infty}^{\infty}\phi_k(t)\phi_j(t)h_e(t_m - t)dt$.

Relation (40) is a quadratic form that can be rewritten in matrix formulation [37]

$$n_{l,\text{ASE–ASE}} = \bar{\mathbf{N}}_\mathbf{l}^\dagger\mathbf{D}\boldsymbol{\Phi}\mathbf{D}\bar{\mathbf{N}}_\mathbf{l} \quad l = r_c,\ r_s,\ p_c,\ p_s \quad (41)$$

where † denotes transpose, $[\mathbf{D}]_{kk} = \sigma_k$ is a diagonal matrix with diagonal elements equal to the standard deviations of $c_{l,k}$, and $\bar{\mathbf{N}}_\mathbf{l}$ is a column vector with elements $[\bar{\mathbf{N}}_\mathbf{l}]_k = \bar{c}_{l,k}$, where $\bar{c}_{l,k}$ are new RVs following a normal distribution.

The quadratic form (41) can be diagonalized using a unitary transformation $\bar{\mathbf{N}}_\mathbf{l} = \mathbf{M}\hat{\mathbf{N}}_\mathbf{l}$, where $\mathbf{M}$ is a transformation matrix whose columns are the eigenvectors of $\mathbf{D}\boldsymbol{\Phi}\mathbf{D}$ and $\hat{\mathbf{N}}_\mathbf{l}$ is a new column vector with elements $[\hat{\mathbf{N}}_\mathbf{l}]_k = \hat{c}_{l,k}$, where $\hat{c}_{l,k}$ are new RVs following a normal distribution. It can be shown that the new RVs $\hat{c}_{l,k}$ are uncorrelated and, thus, independent [61]. Finally, substituting in (41) yields

$$\begin{aligned} n_{l,\text{ASE–ASE}} &= \hat{\mathbf{N}}_\mathbf{l}^\dagger\mathbf{M}^\dagger\mathbf{D}\boldsymbol{\Phi}\mathbf{D}\mathbf{M}\hat{\mathbf{N}}_\mathbf{l} = \sum_{k=1}^{\infty} a_k\hat{c}^2_{l,k} \\ l &= r_c,\ r_s,\ p_c,\ p_s \end{aligned} \quad (42)$$

where a_k are the eigenvalues of $\mathbf{D}\boldsymbol{\Phi}\mathbf{D}$.

Similarly, $n_{l,s\text{-ASE}}$ can be written in series in terms of the new i.i.d. RVs $\hat{c}_{l,k}$

$$n_{l,s\text{-ASE}} = 2A\hat{\mathbf{N}}_\mathbf{l}^\dagger\mathbf{M}^\dagger\mathbf{D}\boldsymbol{\Xi}_\mathbf{l} = 2A\sum_{k=1}^{\infty} b_{l,k}\hat{c}_{l,k} \quad l = r_c, r_s \quad (43)$$

where

$$[\boldsymbol{\Xi}_\mathbf{l}]_k = \int_{-\infty}^{\infty}\bar{E}_{r_l}(t)\phi_k(t)h_e(t_m - t)dt \quad l = c, s. \quad (44)$$

Obviously, $b_{l,k}$ in (43) are multiplication coefficients that depend on the unitary transformation $\mathbf{M}$ and are a function of the projection of the received signal on the orthonormal functions

$\phi_k(t)$. Notice that $b_{l,k}$ depend also on the sampling instant t_m, but this dependence is implied in order to simplify the notation.

From (42) and (43), the characteristic function of the $n_s\text{-ASE}(t_m)$ and $n_{\text{ASE–ASE}}(t_m)$ can be evaluated as

$$\psi_{l,\text{ASE}}(v) = \begin{cases} \prod_{k=1}^{\infty} e^{-\frac{2v^2A^2b_{l,k}^2}{1-2iva_k}}(1-2iva_k)^{-p/2} & l = r_c, r_s \\ \prod_{k=1}^{\infty}(1-2iva_k)^{-p/2} & l = p_c, p_s \end{cases} \tag{45}$$

where p takes the values $p = 1, 2$ in the presence or absence of polarizer, respectively.

The characteristic functions $\psi_{s,t}(\omega)$ for the shot and thermal noises can be readily evaluated [49]

$$\psi_{s,t}(v) = e^{-\frac{\sigma_{s,t}^2 v^2}{2}}. \tag{46}$$

Finally, the conditional characteristic function $\psi_{i_m}(v)$ of i_m is given by

$$\begin{aligned}\psi_{i_m}(v) =& E\left\{e^{ivi_m}\right\} \\ =& e^{\frac{ivR\sigma^2 s_o(t_m)}{2}} e^{-\frac{v^2(\sigma_t^2+\sigma_s^2)}{2}} \prod_{k=1}^{\infty} \frac{e^{-\frac{v^2A^2R\sigma^2\left(b_{r_c,k}^2+b_{r_s,k}^2\right)}{1-2iva_k}}}{(1-2iva_k)^p}.\end{aligned} \tag{47}$$

Appendix B

Analytical Expressions for AWG Router Parameters

The equivalent noise bandwidth of a BPF is defined as

$$B_o = \frac{\int_{-\infty}^{\infty} |H(f)|^2 df}{|H(0)|^2} \tag{48}$$

where $|H(f)|^2$ denotes the equivalent low-pass transmittance of the BPF.

If we neglect the periodicity of the AWG router transmittance, we can evaluate analytically the equivalent noise bandwidth of one AWG router by substitution of (33) in (48) and use of the relationship [3.323(2)] in [62]

$$B_o = \sqrt{\pi} f_c. \tag{49}$$

Notice that, for one AWG router, the equivalent noise bandwidth B_o is slightly larger than the 3-dB bandwidth, which is equal to $B_{3\text{ dB}} = 2\sqrt{\ln 2} f_c$.

The impulse response of N concatenated AWG routers is given by

$$h_c(t) = \int_{-\infty}^{\infty} H_c(f) e^{i2\pi ft} df \tag{50}$$

where $H_c(f)$ is the transfer function of the cascade of N optical MUXs/DMUXs.

By substitution of (33) in (50) and use of the relationship [3.323(2)] in [62], we find

$$h_c(t) = \frac{\omega_c}{\sqrt{2\pi N}} e^{(-\omega_c^2 t^2/2N)} \tag{51}$$

where $\omega_c = 2\pi f_c$.

For the simulation described in Appendix C, the duration of the impulse response (51) is arbitrarily defined as eight times the root-mean-square (rms) width τ_{rms} [63]

$$\tau_{\text{rms}}^2 = \frac{\int_{-\infty}^{\infty} (t-\bar{t})^2 h_c(t) dt}{\int_{-\infty}^{\infty} h_c(t) dt} \tag{52}$$

where $\bar{t}$ is defined as

$$\bar{t} = \frac{\int_{-\infty}^{\infty} t h_c(t) dt}{\int_{-\infty}^{\infty} h_c(t) dt}. \tag{53}$$

It is straightforward to show that $\bar{t} = 0$ and $\tau_{\text{rms}} = \sqrt{N}/\omega_c$.

Appendix C

Implementation of the Semi-Analytic Method

The algorithm for the semianalytic evaluation of the error probability involves several computational steps.

1) Evaluation of the signal waveform at the output of the receiver by noiseless simulation of the the block diagram of Fig. 2(b).
2) Analytical evaluation of the ASE noise psd at the photodiode.
3) Analytical evaluation of the characteristic function of the noise at the output of the receiver for each bit, assuming ideal square-law detection and using an expansion of the ASE noise impingent upon the photodiode in Karhunen–Loève series [42]–[44].
4) Asymptotic evaluation of the pdf of the photocurrent at the output of the receiver for each bit from the corresponding characteristic function using the method of steepest descent [26], [38], [41], [46].
5) Evaluation of the conditional error probability for each bit by numerical integration of the pdf tail.
6) Evaluation of the mean error probability by averaging over the conditional error probabilities for all bits.
7) Finally, numerical minimization of the mean error probability by optimization of the decision threshold.

In the simulation, a pseudorandom sequence with period up to 2^6 is used to modulate the optical signal. This is a de Bruijn sequence [64], i.e., a maximal-length pseudorandom sequence with an additional zero added after the longest string of zeros. Successive iterations with different sequence lengths show that longer sequences increase computing time and provide a negligible increase on accuracy. The optical waveform is assumed NRZ with perfect rise and fall times, zero chirp, and infinite extinction ratio. AWG routers are represented by finite impulse response (FIR) filters. The number of coefficients of each FIR filter is calculated so that the duration of the impulse response is equal to eight times the rms width (see Appendix B). For the evaluation of the effective gain provided by each servo-controlled attenuator, relationship (4) is used. For simplicity, only the signal is considered in the calculation of the average power, since it is assumed it is much higher than the ASE noise power for normal network operating conditions. This will introduce a small error for high error probabilities, where the ASE noise is more important.

Commercially available optically preamplified receivers usually have a narrow tunable optical BPF (e.g., fiber Fabry–Perot with optical bandwidth of the order of $4R_b$ [65]) with an auto-tracking circuit that allows the filter to align its transmission peak with the signal carrier frequency. For simplicity, in the following simulations, it is assumed that the equivalent noise bandwidth of the receiver optical BPF is much wider than the equivalent noise bandwidth of each optical MUX/DMUX. Its sole purpose is to eliminate the periodicity of the ASE spectrum inherent in AWG routers and does not cause additional insertion loss or signal filtering. A fourth-order Bessel LPF with cutoff frequency $0.7R_b$ is used at the receiver.

The optimum sampling instant t_m must be found through a numerical minimization of the error probability. Here, for simplicity, the noiseless eye opening at the output of the receiver is used to determine the optimum sampling instant t_m. The evaluation is performed in two steps. First, the propagation delay τ is calculated by correlation of input and output sequences;. Then, τ_δ is calculated in order to maximize the eye opening. A jitter window around τ_δ, due to the clock recovery circuit, can be assumed.

The evaluation of the equivalent transmittance is done analytically using the recursive relationship (8). The autocorrelation of the ASE noise is evaluated using the inverse fast Fourier transform (FFT) with 1024 points.

For the evaluation of the characteristic function from (23), the coefficients a_k, $b_{r_c,k}$, $b_{r_s,k}$, and $k = 1, \ldots$, are needed. As shown in Appendix A, this requires the numerical solution of the homogeneous Fredholm equation of the second kind (39) [46]. For the quadrature, we use the trapezoidal rule with 64–512 nodes. The thermal and shot noise variances are set to zero.

The evaluation of pdf's from the characteristic function is done using the method of steepest descent. The pdf's computed by the steepest descent method are in excellent agreement with the pdf's given by the FFT of the characteristic function.

The optimum threshold occurs at the intersection of the sum of pdf's of the ZEROs and the sum of pdf's of ONEs of the de Bruijn sequence. The optimum threshold is evaluated numerically.

The evaluation of conditional error probabilities directly from the characteristic function using (29) is oscillatory, unless a successful guess of the vicinity of the root v_0 is found. Therefore, numerical integration of the pdf tail is preferable.

ACKNOWLEDGMENT

The authors would like to thank Dr. L. D. Garrett for providing the measurements of Fig. 3, Drs. S. F. Habiby, N. N. Khrais, A. F. Elrefaie, J. B. D. Soole, J. C. Cartledge, S. P. Burtsev, M. Lee, I. Tomkos, and A. Boscovic for helpful discussions, and Ms. L. M. Szemiot for corrections in the syntax of the manuscript.

REFERENCES

[1] R. E. Wagner, R. C. Alferness, A. A. M. Saleh, and M. S. Goodman, "MONET: Multiwavelength optical networking," *J. Lightwave Technol.*, vol. 14, no. 6, pp. 1349–1355, June 1996.

[2] C. S. Li, F. F. K. Tong, K. Liu, and D. G. Messerschmitt, "Channel capacity optimization of chirp-limited dense WDM/WDMA systems using OOK/FSK modulation and optical filters," *J. Lightwave Technol.*, vol. 10, no. 8, pp. 1148–1161, Aug. 1992.

[3] F. Testa, S. Merli, and P. Pagnan, "Fabry-perot filter bandwidth effects on end to end transmission performances in a multiwavelength transport network," *IEEE Photon. Technol. Lett.*, vol. 6, pp. 1027–1030, Aug. 1994.

[4] N. N. Khrais, A. F. Elrefaie, R. E. Wagner, and S. Ahmed, "Performance degradation of multiwavelength optical networks due to laser and (de)multiplexers misalignments," *IEEE Photon. Technol. Lett.*, vol. 7, pp. 1348–1350, Nov. 1995.

[5] ——, "Performance of cascaded misaligned optical (de)multiplexers in multiwavelength optical networks," *IEEE Photon. Technol. Lett.*, vol. 8, pp. 1073–1075, Aug. 1996.

[6] C. Caspar, H. M. Foisel, R. Freund, U. Krüger, and B. Strebel, "Cascadability of array-waveguide grating (de)multiplexers in transparent optical networks," in *Proc. Optical Fiber Communication Conf.*, vol. TuE2, Dallas, TX, Feb. 1997, pp. 19–20.

[7] H. Miyata, H. Onaka, K. Otsuka, and T. Chikama, "Bandwidth and ripple requirements for cascaded optical (de)multiplexers in multiwavelength optical networks," in *Optical Fiber Communication Conf.*, vol. TuE3, Dallas, TX, Feb. 1997, pp. 20–21.

[8] I. Roudas, N. Antoniades, R. E. Wagner, S. F. Habiby, and T. E. Stern, "Influence of filtered ase noise and optical filter shape on the performance of a WADM cascade," in *Proc. Eur. Conf. Optical Communications*, vol. 2, Edinburgh, U.K., Sept. 1997, pp. 143–146.

[9] B. J. Eggleton, G. Lenz, N. Litchinitser, D. B. Patterson, and R. E. Slusher, "Implications of fiber grating dispersion for WDM communication systems," *IEEE Photon. Technol. Lett.*, vol. 9, pp. 1403–1405, Oct. 1997.

[10] I. Roudas, N. Antoniades, R. E. Wagner, and L. D. Garrett, "Influence of realistic optical filter characteristics on the performance of multiwavelength optical networks," in *Proc. IEEE/LEOS Annu. Meeting*, vol. 2, Nov. 1997, pp. 542–543.

[11] C. Caspar, H. M. Foisel, R. Freundand, and B. Strebel, "Four-channel 10 Gb/s transmission over 15-wavelength-selective cross-connect paths and 1175 -km dispersion compensated standard single-mode fiber links," in *Proc. Optical Fiber Communication Conf.*, vol. ThP3, San Jose, CA, Feb. 1998, pp. 327–329.

[12] N. M. Litchinitser, B. J. Eggleton, and G. P. Agrawal, "Dispersion of cascaded fiber gratings in WDM lightwave systems," *J. Lightwave Technol.*, vol. 16, no. 8, pp. 1523–1529, Aug. 1998.

[13] T. Otani, N. Antoniades, I. Roudas, and T. E. Stern, "Cascadability of passband-flattened arrayed waveguide-grating filters in WDM optical networks," *IEEE Photon. Technol. Lett.*, vol. 11, pp. 1414–1416, Nov. 1999.

[14] M. Kuznetsov, N. M. Froberg, S. R. Henion, and K. A. Rauschenbach, "Power penalty for optical signals due to dispersion slope in WDM filter cascades," *IEEE Photon. Technol. Lett.*, vol. 11, pp. 1411–1413, Nov. 1999.

[15] H. Bock, P. Leisching, A. Richter, D. Stoll, and G. Fischer, "System impact of cascaded optical add/drop multiplexers based on tunable fiber Bragg gratings," in *Proc. Optical Fiber Communication Conf.*, vol. WM29, Baltimore, MD, 2000, pp. 296–298.

[16] K. P. Ho, L. K. Chen, and F. Tong, "Modeling of waveform distortion due to optical filtering," *IEEE J. Select. Topics Quantum Electron.*, vol. 6, pp. 223–226, Mar./Apr. 2000.

[17] H. Bock, G. Mohs, C. Furst, H. Geiger, and G. Fischer, "Impact of optical demultiplexers on DWDM transmission of 40 Gb/s channels," in *Proc. Eur. Conf. Optical Communications*, vol. 16, Munich, Germany, Aug. 2000, p. 3.

[18] I. Tomkos, R. Hesse, N. Antoniades, and A. Boskovic, "Impact of filter concatenation on the performance of metropolitan area networks utilizing directly modulated lasers," in *Proc. Optical Fiber Communication Conf.*, vol. WBB4, Anaheim, CA, Mar. 2001.

[19] F. Shehadeh, T. Suzaki, J. C. Chiao, K. P. Ho, S. K. Liaw, and R. S. Vodhanel, "Impact of external modulator in an eight-wavelength eight-node WDM ring network," in *Proc. Optical Fiber Communication Conf.*, vol. TuE4, Dallas, TX, Feb. 1997, pp. 21–22.

[20] M. Nissov, R. J. S. Pedersen, and B. F. Jorgensen, "Transmission performance through cascaded 1-nm arrayed waveguide multiplexers at 10 Gb/s," *IEEE Photon. Technol. Lett.*, vol. 9, pp. 1038–1040, Jul. 1997.

[21] C. Caspar, H. M. Foisel, C. v. Helmolt, B. Strebel, and Y. Sugaya, "Comparison of cascadability of different types of commercially available wavelength (de)multiplexers," *Electron. Lett.*, vol. 33, no. 19, pp. 1624–1625, Sept. 1997.

[22] K. Liu and W. K. Wang, "Misalignment distortion penalty in moderate-speed directly modulated WDM systems and its reduction using fiber Bragg grating lasers," *IEEE Photon. Technol. Lett.*, vol. 9, pp. 1649–1651, Dec. 1997.

[23] G. Nykolak, B. J. Eggleton, G. Lenz, and T. A. Strasser, "Dispersion penalty measurements of narrow fiber Bragg gratings at 10 Gb/s," *IEEE Photon. Technol. Lett.*, vol. 10, pp. 1319–1321, Sept. 1998.

[24] H. Maeda, Y. Tada, M. Sumida, S. Saito, and Y. Hayashi, "Performance degradation of long-distance optical WDM networks due to bandwidth limitations of wavelength multiplexers and demultiplexers," *IEEE Photon. Technol. Lett.*, vol. 11, pp. 1509–1511, Nov. 1999.

[25] M. C. Jeruchim, "Techniques for estimating the bit error rate in the simulation of digital communication systems," *IEEE J. Select. Areas Commun.*, vol. SAC-2, pp. 153–170, Jan. 1984.

[26] C. W. Helstrom, "Distribution of the filtered output of a quadratic rectifier computed by numerical contour integration," *IEEE Trans. Inform. Theory*, vol. IT-32, pp. 450–463, Jul. 1986.

[27] P. S. Henry, "Error-rate performance of optical amplifiers," in *Proc. Optical Fiber Communication Conf.*, vol. THK3, Houston, TX, 1989, pp. 170–170.

[28] D. Marcuse, "Derivation of analytical expressions for the bit-error probability in lightwave systems with optical amplifiers," *J. Lightwave Technol.*, vol. 8, no. 12, pp. 1816–1823, Dec. 1990.

[29] ——, "Calculation of bit-error probability for a lightwave system with optical amplifiers and post-detection Gaussian noise," *J. Lightwave Technol.*, vol. 9, no. 4, pp. 505–513, Apr. 1991.

[30] F. Abramovich and P. Bayvel, "Some statistical remarks on the derivation of ber in amplified optical communication systems," *IEEE Trans. Commmun.*, vol. 45, pp. 1032–1034, Sept. 1997.

[31] P. A. Humblet and M. Azizoglu, "On the bit error rate of lightwave systems with optical amplifiers," *J. Lightwave Technol.*, vol. 9, no. 11, pp. 1576–1582, Nov. 1991.

[32] J.-S. Lee and C.-S. Shim, "Bit-error-rate analysis of optically preamplified receivers using an eigenfunction expansion method in optical frequency domain," *J. Lightwave Technol.*, vol. 12, no. 7, pp. 1224–1229, Jul. 1994.

[33] L. F. B. Ribeiro, J. R. F. D. Rocha, and J. L. Pinto, "Performance evaluation of edfa preamplified receivers taking into account intersymbol interference," *J. Lightwave Technol.*, vol. 13, no. 2, pp. 225–232, Feb. 1995.

[34] S. R. Chinn, "Error-rate performance of optical amplifiers with fabry-perot filters," *Electron. Lett.*, vol. 31, no. 9, pp. 756–757, Apr. 1995.

[35] D. Ben-Eli, Y. E. Dallal, and S. S. Shitz, "Performance bounds and cutoff rates of quantum limited ook with optical amplification," *IEEE J. Select. Areas Commun.*, vol. 13, pp. 510–530, Apr. 1995.

[36] S. L. Danielsen, B. Mikkelsen, T. Durhuus, C. Joergensen, and K. E. Stubkjaer, "Detailed noise statistics for an optically preamplified direct detection receiver," *J. Lightwave Technol.*, vol. 13, no. 5, pp. 977–981, May 1995.

[37] C. Lawetz and J. C. Cartledge, "Performance of optically preamplified receivers with fabry-perot optical filters," *J. Lightwave Technol.*, vol. 14, no. 11, pp. 2467–2474, Nov. 1996.

[38] I. T. Monroy and G. Einarsson, "Bit error evaluation of optically preamplified direct detection receivers with fabry-perot optical filters," *J. Lightwave Technol.*, vol. 15, no. 8, pp. 1546–1553, Aug. 1997.

[39] S. Herbst, P. Meissner, M. Baussmann, and M. Erbasch, "Sensitivity of a direct WDM-system with a frequency selective optical receiver and optical preamplifier," *J. Lightwave Technol.*, vol. 16, no. 1, pp. 32–36, Jan. 1998.

[40] G. Jacobsen, K. Bertilsson, and Z. Xiaopin, "WDM transmission system performance: Influence of non-Gaussian detected ASE noise and periodic DEMUX characteristic," *J. Lightwave Technol.*, vol. 16, no. 10, pp. 1804–1812, Oct. 1998.

[41] E. Forestieri, "Evaluating the error probability in lightwave systems with chromatic dispersion, arbitrary pulse shape and pre- and postdetection filtering," *J. Lightwave Technol.*, vol. 18, no. 11, pp. 1493–1503, Nov. 2000.

[42] H. Van Trees, *Detection, Estimation and Modulation Theory*. New York: Wiley, 1968, vol. 1.

[43] W. B. Davenport Jr and W. L. Root, *An Introduction to the Theory of Random Signals and Noise*. Piscataway, NJ: IEEE Press, 1987.

[44] C. W. Helstrom, *Statistical Theory of Signal Detection*, 2nd ed. Tarrytown, NY: Pergamon Press, 1968.

[45] R. Courant and D. Hilbert, *Methods of Mathematical Physics*. New York: Wiley, 1989, vol. 1.

[46] G. Arfken, *Mathematical Methods for Physicists*, 3rd ed. New York: Academic, 1985.

[47] I. Roudas, D. H. Richards, N. Antoniades, J. L. Jackel, and R. E. Wagner, "An efficient simulation model of the erbium-doped fiber for the study of multiwavelength optical networks," *Opt. Fiber Technol.*, vol. 5, no. 4, pp. 363–389, Oct. 1999.

[48] I. Roudas, N. Antoniades, D. H. Richards, R. E. Wagner, J. L. Jackel, S. F. Habiby, T. E. Stern, and A. F. Elrefaie, "Wavelength-domain simulation of multiwavelength optical networks (invited paper)," *IEEE J. Select. Topics Quantum Electron.*, vol. 6, pp. 348–362, Mar./Apr. 2000.

[49] J. G. Proakis, *Digital Communications*, 3rd ed. New York: McGraw-Hill, 1995.

[50] G. P. Agrawal, *Fiber-Optic Communication Systems*, 2nd ed. New York: Wiley, 1992.

[51] S. Benedetto, E. Biglieri, and V. Castellani, *Digital Transmission Theory*. Englewood Cliffs, NJ: Prentice-Hall, 1987.

[52] M. Abramowitz and I. A. Stegun, *Handbook of Mathematical Functions*. New York: Dover, 1972.

[53] I. P. Kaminow and T. L. Koch, Eds., *Optical Fiber Telecommunications IIIB*. New York: Academic, 1997.

[54] C. Dragone, "Efficient techniques for widening the passband of a wavelength router," *J. Lightwave Technol.*, vol. 16, no. 10, pp. 1895–1906, Oct. 1998.

[55] O. Ishida and H. Takahashi, "Loss-imbalance equalization in arrayed-waveguide-grating (AWG) multiplexer cascades," *J. Lightwave Technol.*, vol. 13, no. 6, pp. 1155–1163, June 1995.

[56] H. Takahashi, K. Oda, H. Toba, and Y. Inoue, "Transmission characteristics of arrayed-waveguide $N \times N$ wavelength multiplexer," *J. Lightwave Technol.*, vol. 13, no. 3, pp. 447–455, Mar. 1995.

[57] B. Fondeur, R. Cella, and C. Nicolas, "Effect of process variations on arrayed waveguide grating dispersion," in *Proc. Eur. Conf. Optical Communications*, Nice, France, Sept. 1999, pp. I328–329.

[58] J. Gehler and K. Lösch, "Dispersion measurement of arrayed waveguide gratings by fourier-transform spectroscopy," in *Proc. Eur. Conf. Optical Communications*, Nice, France, Sept. 1999, pp. I368–369.

[59] W. Idler, S. Bigo, Y. Frignac, B. Franz, and G. Veith, "Vestigial side band filtering for ultra high capacity (0.64 bit/s/Hz) transmission of 128×40 Gb/s channels," in *Proc. Optical Fiber Communication Conf.*, vol. MM3, Anaheim, CA, 2001.

[60] S. Bigo, Y. Frignac, G. Sarlet, S. Borne, P. Tran, C. Simonneau, D. Bayard, A. Jourdan, J. P. Hamaide, W. Idler, R. Dischler, G. Veith, H. Gross, and V. Poehlmann, "10.2 Tb/s 256×42.7 Gb/s PDM/WDM) transmission over 100 km teralight fiber with 1.28 b/s/Hz spectral efficiency," in *Proc. Optical Fiber Communication Conf.*, vol. PD25, Anaheim, CA, 2001.

[61] M. Schwartz, W. R. Bennett, and S. Stein, *Communication Systems and Techniques*. New York: McGraw-Hill, 1966.

[62] I. S. Gradshteyn and I. M. Ryzhik, *Tables of Integrals, Series, and Products*. New York: Academic, 1981.

[63] B. E. A. Saleh and M. C. Teich, *Fundamentals of Photonics*. New York: Wiley, 1991.

[64] S. W. Golomb, *Shift Register Sequences*. San Francisco, CA: Holden-Day, 1967.

[65] Y. K. Park and S. W. Granlund, "Optical preamplifier receivers: Application to long-haul digital transmission," *Opt. Fiber Technol.*, vol. 1, no. 1, pp. 59–71, Oct. 1994.

I. Roudas (M'00), photograph and biography not available at the time of publication.

N. Antoniades (S'91–M'92), photograph and biography not available at the time of publication.

T. Otani, photograph and biography not available at the time of publication.

T. E. Stern (S'54–M'57–SM'67–F'72–LF'95), photograph and biography not available at the time of publication.

R. E. Wagner (S'84–M'85), photograph and biography not available at the time of publication.

D. Q. Chowdhury (S'89–M'89), photograph and biography not available at the time of publication.